Dual-Targeting Sulfamethoxazole Derivatives Overcome Multidrug Resistance in ESKAPE Pathogens by Inhibiting Quorum Sensing and Efflux Pumps

Benedicta Yayra Adzah[1], Prince Danan Biniyam[1], Victoria Ohene-Adu[1], Michael Osei[1], Kwabena Adu-Adjei[1], Victoria Elmes[2], Iain Goodall[2], Vuvor Faustina[1], , Yvonne Dogbeda Agboyibor[1], Patrick Gyan[1], Paul Quansah[1], Cyril Makafui Amengor[3], Joshua Boateng [2], En Zhang[4], Maxwell Ampomah-Wireko[5] , Ernest Oyeh[6] , Cedric Dzidzor Kodjo Amengor[1*],

[1] Department of Pharmaceutical Chemistry, Drug Discovery Unit, School of Pharmacy, University of Health and Allied Sciences, Ho, Ghana; [2] School of Science, University of Greenwich, United Kingdom. [3]Department of Mathematics, University of Ghana, Legon-Ghana.

[4]School of Pharmaceutical Sciences, Key Laboratory of Advanced Pharmaceutical Technology, Ministry of Education of China, Zhengzhou University, Zhengzhou 450001, PR China

[5]School of Pharmaceutical Sciences, Key Laboratory of Advanced Pharmaceutical Technology, Ministry of Education of China, Zhengzhou University, Zhengzhou 450001, PR China

[6]Department Of Nursing, Faculty Of Science, Methodist University Ghana, Ghana.

Corresponding Author: Department of Pharmaceutical Chemistry, School of Pharmacy, University of Health and Allied Sciences, Ho. camengor@uhas.edu.gh. Contact: +233246456764.

Abstract:

The rapid emergence of pan-drug-resistant pathogens necessitates innovative antimicrobial strategies that overcome conventional resistance. This study reports the structure-guided design of sulfamethoxazole derivatives as dual inhibitors of quorum sensing (LasR) and efflux pumps (AcrB), alongside the classic dihydropteroate synthase (DHPS) target. High-throughput virtual screening of 54 derivatives, followed by MM-GBSA analysis, prioritized five novel compounds for synthesis. Their structures were confirmed by $^{1}H/^{13}C$ NMR, FT-IR, and mass spectrometry. All compounds demonstrated potent growth inhibition (MICs 15.625–125 μg/mL) against *Proteus mirabilis*, *Salmonella typhi*, and *Escherichia coli*, though activity against the more resistant *Pseudomonas*

aeruginosa was reduced. Critically, lead compounds SMX033 and SMX015 achieved >99% biofilm inhibition against *P. mirabilis*, and SMX033 showed significant efflux pump inhibition, directly validating our *in silico* predictions of a multi-target mechanism. In particular, compound SMX 033 exhibited the best antimicrobial activity and lowest cytotoxicity of all the sulfamethoxazole derivatives with a CCC_{50} value of 286.20 µM against *Vero cells*. Despite predicted *in silico* genotoxicity, these derivatives provide a promising chemical scaffold for combating multidrug-resistant infections by concurrently attenuating virulence and restoring antibiotic susceptibility.

Keywords: Sulfamethoxazole derivatives, antimicrobial resistance, ESKAPE pathogens

1.0 Introduction

Bacterial-related infectious diseases pose a significant threat to global health due to their clinical diversity, high transmissibility, and the rapid emergence of antibiotic-resistant strains [1]. These infections are the leading causes of morbidity and mortality worldwide [2]. Antimicrobial resistance is a pressing global concern, as microorganisms develop resistance to existing antibiotics, rendering many treatments ineffective [3, 4]. This highlights the urgent need for novel antimicrobial agents with broad-spectrum efficacy, particularly against multidrug-resistant strains.

Heterocyclic compounds have become a cornerstone in medicinal chemistry because of their potential versatile pharmacological activities [1]. Therefore, synthetic medicinal chemists usually introduce a heterocyclic moiety, representing 85%, in the design of most drugs in order to enhance pharmacological activity while addressing metabolism and pharmacokinetic issues [2, 3]. Despite their ease of synthesis, the heterocyclic core imparts the clinical drug candidate with suitable pharmacokinetic properties [4]. Most drugs fail to move from the bench to the patient because of poor pharmacokinetic profiles; therefore, the introduction of the heterocyclic groups can contribute to reducing the attrition rate of promising clinical candidates while improving the efficacy and toxicity profiles [5].

The isoxazole class of heterocyclics continues to make an immense contribution to the drug discovery pipeline with the introduction of drugs possessing anti-inflammatory, antimicrobial, antioxidant, and other anti-infective properties [6, 7]. Drugs that possess the isoxazole group include sulfamethoxazole, sulfisoxazole, flucloxacillin, valdecoxib, leflunomide, and isoxicam [8, 9] (Figure 1). One of the most common and clinically useful sulphonamides, sulfamethoxazole is an antimicrobial drug used in combination with trimethoprim for the treatment of bacteria-related

infections [10, 11]. It has established activity against Gram-positive and Gram-negative organisms, rendering it a broad-spectrum antibiotic, but it is gradually losing potency due to antimicrobial resistance [12]. Current studies have demonstrated that sulfamethoxazole derivatives possess antimicrobial properties, and they represent promising clinical candidates. These include sulfamethoxazole ligand metal complexes, which showed potency against some ESKAPE pathogens (*Staphylococcus aureus*, *Escherichia coli*, and *Klebsiella pneumoniae*) and fungal strains of Aspergillus, and these complexes have the ability to inhibit bacterial biofilm formation [13, 14]. They have also been shown to inhibit the growth of virulent forms of *Mycobacteria* by blocking biofilm formation and efflux pumps of the bacteria.

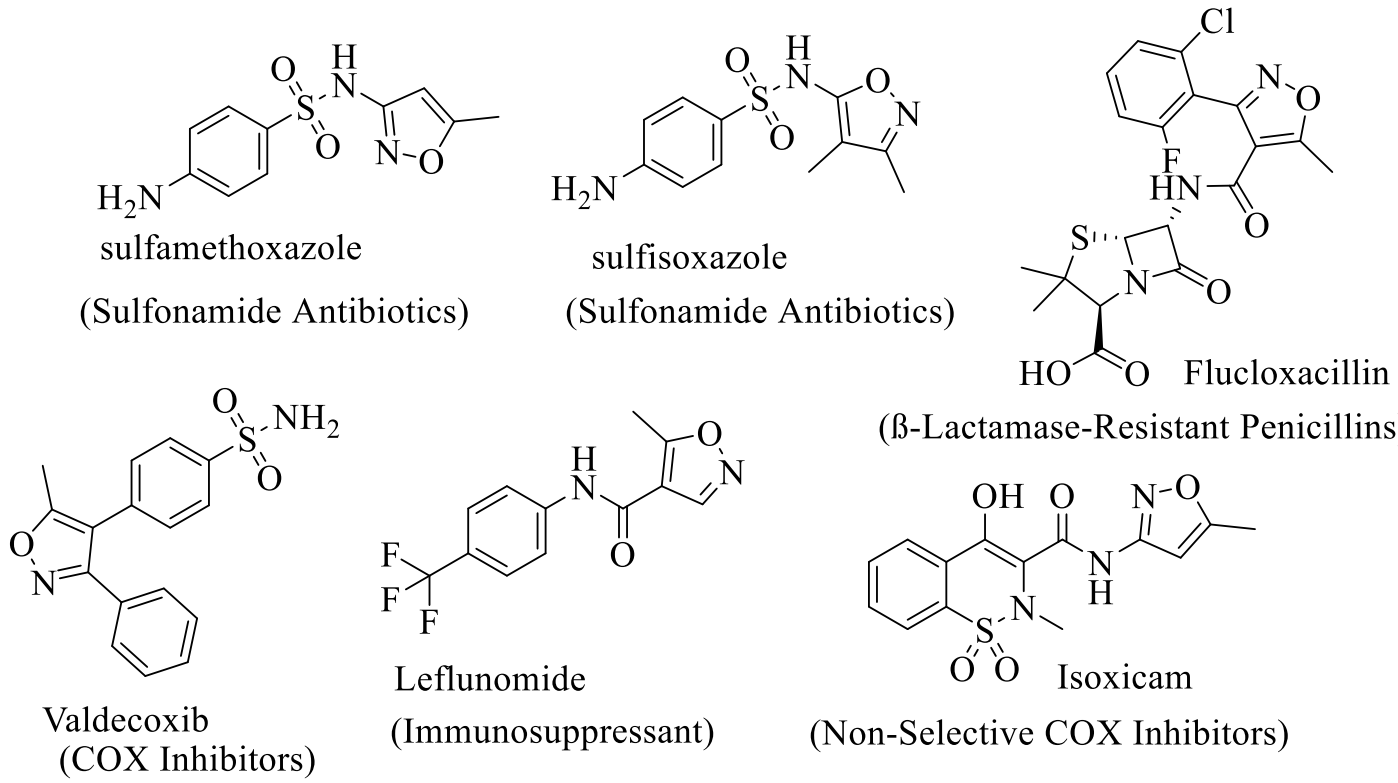

Figure 1. Some isoxazole containing biological active heterocyclic compounds.

Sulfonamides inhibit the para-amino benzoic acid (PABA) pathway, blocking folate synthesis required for DNA replication. However, the approach of drug discovery through targeting this bacteria mechanism is no longer effective due to antibiotic resistance [15, 16]. Moreover, the development of multi-drug resistance to sulfamethoxazole has also been attributed to mutation and generation of new resistance genes, quorum sensing, biofilm formation, presence of efflux pumps, and redundancy of the known inhibitory pathways [17, 18, 19]. This has rendered the drug sulfamethoxazole/trimethoprim (co-trimoxazole) ineffective as the first choice of drug for the treatment of most infections.

The application of computational methods such as molecular docking and molecular dynamics simulations has greatly enhanced our understanding of how sulfamethoxazole derivatives interact with biological targets such as DHPS [20]. These approaches provide high-resolution information about binding affinities, conformational dynamics, and molecular recognition [21]. This combination of computational and experimental approaches has become an important part of current drug development, allowing for the rapid identification and optimization of new sulfamethoxazole compounds with enhanced pharmacological characteristics [22, 23, 24].

In this current study, we employed a computationally guided approach to design a library of sulfamethoxazole derivatives targeting DHPS, LasR, and AcrB, and to explore their resulting potential new phenotypic antibacterial, efflux pump inhibitory, and biofilm inhibitory activities.

2.0 Experimental design

The study involved 54 sulfamethoxazole derivatives, with sulfamethoxazole as a benchmark drug [25]. Ligands were designed using positional isomerization of 19 diverse substituents, electron donating (dimethylamino, hydroxy, methoxy, ethoxy, methylthio, methyl, acetamido), electron withdrawing (nitro, cyano, trifluoromethyl, carboxylic acid, methyl ester, sulfonic acid, formyl), and halogens (bromo, chloro, fluoro), on the aromatic ring of the sulfamethoxazole (SMX) core. Molecular docking and MMGBSA calculations were performed separately on DHPS, LasR, and AcrB proteins to estimate binding free energy. Five sulfamethoxazole derivatives were prioritized for synthesis from the *in silico* screening and antimicrobial evaluation, focusing on synthetic accessibility, structural diversity, and resource efficiency.

3.0 Chemistry

The chemicals used for the synthesis were purchased from Merck® (Gillingham, UK) and were of analytical grade, except for the HPLC-grade solvents (methanol and acetonitrile) sourced from Fischer Scientific (Loughborough, UK). The progress of the reaction and the purity of the synthesized compounds were monitored by thin-layer chromatography (TLC) using aluminum plates pre-coated with silica gel, observed at a fluorescence wavelength of 254 nm. A calibrated pH meter (Eutech Instruments ECPH70042GS, Singapore) was employed to monitor the pH, which in turn offered information about the progress of the reaction. The purity of the compounds was further assessed by determining their melting points using a B-540 analyzer for melting points (Büchi Corporation, New Castle, DE, USA), and the reported melting points are uncorrected. The presence of key functional groups in the synthesized compounds was recorded using a Perkin–

Elmer Spectrum 100 FT–IR spectrometer (Perkin–Elmer Inc., Waltham, MA, USA) equipped with attenuated total reflectance mode. NMR spectra were acquired on a Bruker Ascend III (500 MHz) spectrometer (Bruker BioSpin AG, Fällanden, Switzerland). Chemical shifts were reported in parts per million (δ) relative to tetramethylsilane (TMS), with the residual solvent serving as the lock solvent ([D6] DMSO, δ = 2.50 ppm for 1H and δ = 39.52, 77.5 ppm for 13C). High-resolution mass spectra were obtained using an HPLC (Shimadzu LC-2010A) in conjunction with a time-of-flight (quadrupole mass analyzer) mass spectrometer operating in positive ESI ionization mode.

3.1 General procedure for the synthesis of the sulfamethoxazole hybrids [25]

A mixture of 3-amino-5-methylisoxazole (2.5 mmol, 1 equiv.) and substituted sulfonyl chlorides (2.5 mmol, 1.0 equiv.) was suspended in 30 mL of water. The pH of the suspension was adjusted and maintained at 8.0 by adding a 1M Na_2CO_3 aqueous solution at room temperature and monitored using a pH meter probe. The progress of the reaction was tracked using TLC with a developing solvent of (CH_2Cl_2):(Et_2O) [60:40]. Upon completion of the reaction, concentrated HCl was added slowly to lower the pH to 2.0. The resulting precipitate was collected by suction filtration, washed with water, and dried to yield the crude compound. The crude product was purified by silica column chromatography using a dichloromethane (CH_2Cl_2): diethyl ether (Et_2O) [60:40] mobile phase through gradient elution to isolate the target compounds as solid products.

3.2 Spectral data

N-(5-methylisoxazol-3-yl)-2-nitrobenzenesulfonamide (SMX001)

White solid. Yield (0.482 g, 52 %), m.p. 116-118 °C; R_f: 0.75, FT-IR (ν/cm): 2952, 2831, (aliphatic –CH), 1649 (-C=O), 1566 (-C=C<u>H</u>-), 822, 798, 524 (Ar-C-H), ^{1}H NMR (400 MHz, $CDCl_3$ δ ppm) , 8.12 (2H, m, −ArH), 7.86 (1H, m, −ArH), 7.75 (1H, m, −ArH), 6.17 (1H, q, −ArN<u>H</u> $_{isox}$), 2.95 (br, 1H, s, −$NHSO_2$−), 2.36 (3H, d, J= 4.00 Hz −$ArCH_3$); ^{13}C NMR (400 MHz, $CDCl_3$ δ ppm) δ; 171.04, 156.97, 134.44, 132.79, 132.60, 131.45, 125.38, 96.02, 12.67; HRMS (ESI): *m/z* calculated for $C_{10}H_9N_3O_5S$: 283.0263, found, $[M+H]^+$: 284.0327.

N-(5-methylisoxazol-3-yl)-4-nitrobenzenesulfonamide (SMX003)

Beige solid. Yield (0.482 g, 68 %), m.p. 118-120 °C; R_f: 0.75, FT-IR (ν/cm): 2952, 2831, (aliphatic –CH), 1649 (-C=O), 1566 (-C=C<u>H</u>-), 822, 798, 524 (Ar-C-H), ^{1}H NMR (400 MHz, $CDCl_3$ δ ppm) , 8.34 (2H, d. J= 8.00, −ArH), 8.08 (2H, d, J= 8.00, −ArH), 7.13 (1H, m, −ArH), 6.18-6.17 (1H, q, −ArN<u>H</u> $_{isox}$), 2.56 (br, 1H, s, −$NHSO_2$−), 2.36-2.35 (3H, d, J= 4.00 Hz −$ArCH_3$); ^{13}C NMR

(400 MHz, $CDCl_3$ δ ppm) δ; 171.17, 157.20, 145.12, 128.49, 124.47, 95.56, 50.20, 48.92, 49.78, 29.73, 12.67; HRMS (ESI): *m/z* calculated for $C_{10}H_9N_3O_5S$: 283.0263, found, $[M+H]^+$: 284.0329.

Methyl 4-(N-(5-methylisoxazol-3-yl) sulfamoyl)benzoate (SMX015)

Beige solid. Yield (0.5493 g, 75 %), m. p. 126-129 °C; R_f: 0.65, FT-IR (ν/cm): 2952, 2831, (aliphatic –CH), 1649 (-C=O), 1566 (-C=C<u>H</u>-), 822, 798, 524 (Ar-C-H), ^{1}H NMR (400 MHz, $CDCl_3$ δ ppm) 8.48 (br, 1H, s, −$NHSO_2$−), 8.15 (2H, d, *J*= 8.00 Hz, −ArH), 7.91 (2H, d, J = 8.00 Hz, −ArH), 6.26-6.24 (1H, q, −Ar<u>N</u>H $_{isox}$), 3.95 (3H, s, −OCOC<u>H</u>$_3$), 2.31 (3H, s, −$ArCH_3$) ^{13}C NMR (400 MHz, $CDCl_3$ δ ppm) δ; δ; 171.38, 165.37, 142.67 134.64, 130.49, 127.13, 95.55, 52.74, 21.60, 12.73; HRMS (ESI): *m/z* calculated for $C_{12}H_{12}N_2O_5S$: 296.0567, found, $[M+H]^+$:297.0535.

2-bromo-N-(5-methylisoxazol-3-yl) benzenesulfonamide (SMX019)

Pale brown solid. Yield (0.550 g, 71 %), m.p. 164-167 °C; R_f: 0.66, FT-IR (ν/cm): 2952, 2831, (aliphatic –CH), 1649 (-C=O), 1566 (-C=C<u>H</u>-), 822, 798, 524 (Ar-C-H), ^{1}H NMR (400 MHz, $CDCl_3$ δ ppm) 8.56 (br, 1H, s, −$NHSO_2$−), 8.13 (1H, m, −ArH), 7.45 (1H, m, −ArH), 7.13-7.18 (2H, d, *J*= 8.00 Hz, −ArH), 6.11-6.10 (1H, q, −ArH $_{isox}$), 2.31 (3H, s, −$ArCH_3$) ; ^{13}C NMR (400 MHz, $CDCl_3$ δ ppm) δ; 171.01, 156.67, 138.03, 135.50, 134.56, 131.56, 127.79, 120.20, 95.27, 12.68; HRMS (ESI): *m/z* calculated for $C_{10}H_9{}^{35}B_rN_2O_3S$: 315.9517, found, $[M+H]^+$: 316.9591; calculated for $C_{10}H_9{}^{37}B_rN_2O_3S$: 316.9517, found, $[M+2]^+$: 318.9565.

4-methyl-N-(5-methylisoxazol-3-yl) benzenesulfonamide (SMX033)

Beige solid. Yield (0.4110 g, 65 %), m.p. 125-127 °C; R_f: 0.52, FT-IR (ν/cm): 2952, 2831, (aliphatic –CH), 1649 (-C=O), 1566 (-C=C<u>H</u>-), 822, 798, 524 (Ar-C-H), ^{1}H NMR (400 MHz, $CDCl_3$ δ ppm) 8.24 (br, 1H, s, −$NHSO_2$−), 7.74-7.72 (2H, d, J = 8.00 Hz, −ArH), 7.70-7.68 (1H, d, J = 8.00 Hz, −ArH), 6.26-6.24 (1H, q, −Ar<u>N</u>H $_{isox}$), 2.40 (3H, s, −$ArCH_3$), 2.37-2.36 (3H, d, J= 4.00m −$ArCH_3$) ^{13}C NMR (400 MHz, $CDCl_3$ δ ppm) δ 171.01, 157.53, 144.56, 136.02, 129.92, 127.10, 95.55, 21.60, 12.73; HRMS (ESI): *m/z* calculated for $C_{11}H_{12}N_2O_3S$: 252.0569, found, $[M+H]^+$:253.0649.

4.0 Antimicrobial assay

4.1 Minimum inhibitory concentration assay

To determine the minimum inhibitory concentration (MIC), the micro-well dilution method outlined by Fetse *et al.* (2014) and Agyare *et al.* (2013) was used [26, 27]. This approach measures the development/growth of microorganisms at different antimicrobial concentrations. Aqueous

solutions of the compounds were prepared at a concentration of 200 mg/mL by dissolving 0.6 g of each synthesized compound in 3 mL of sterile water. In 96-well plates, 100 μL of double-strength broth was added to each well, followed by the addition of the compounds at a series of doubling dilutions, with final concentrations ranging from 250 to 3.91 μg/mL. The test organisms, standardized to an inoculum size of 1 x 10^6 CFU/mL using the 0.5 M MacFarland standard, were then added to each well at a volume of 20 μL. The plates were covered and incubated at 37°C for 24 hours. After the incubation period, 25 μL of 1.25 mg/mL of 3-(4,5-dimethylthiazol-2-yl)-2,5-diphenyltetrazolium bromide (MTT) solution was added to each well and further incubated at 37°C for 30 minutes. The MIC was determined as the lowest concentration at which no visible change in colour from yellow to purple occurred following the addition of MTT, indicating no microbial growth.

4.2 Crystal violet biofilm inhibition assay

The biofilm inhibitory activity against *Proteus mirabilis*, *Salmonella typhi*, *Escherichia coli*, and *Pseudomonas aeruginosa* was evaluated using a modified assay that retains crystal violet, adapted from Ofori et al. (2021) [28]. Bacterial cultures were grown on brain heart infusion (BHI) agar at 37°C for 24 hours. Colonies were suspended in BHI broth and adjusted to 0.5 McFarland standard ($\sim 1.5 \times 10^8$ CFU/mL) using sterile saline. In sterile 96-well plates, 100 μL of standardized bacterial suspension was combined with 100 μL of BHI broth containing test compounds at final sub-MIC concentrations. Wells containing bacteria without compounds served as growth controls, while wells with BHI broth alone served as blanks. Plates were wrapped in aluminum foil and incubated statically at 37°C for 24 hours. After incubation, planktonic cells were aspirated, and wells were washed three times with 200 μL phosphate-buffered saline (PBS, pH 7.4) to remove non-adherent cells. Adherent biofilms were fixed with 150 μL methanol for 15 minutes, stained with 0.1% (w/v) crystal violet for 15 minutes, and washed three times with distilled water. Bound dye was solubilized with 150 μL of 95% ethanol for 30 minutes. Absorbance was measured at 630 nm using a microplate reader (BioTek Synergy H1, USA). Percentage biofilm inhibition was calculated as:

$$\text{Inhibition (\%)} = 1 - \frac{ODtest - ODblank}{ODgrowthcontrol - ODblank} \times 100$$

Each compound-pathogen combination was tested in triplicate wells across three independent experiments.

4.3 Ethidium bromide efflux pump inhibition assay

Efflux pump inhibition was assessed against *P. mirabilis*, *S. typhi*, *E. coli*, and *P. aeruginosa* using an ethidium bromide accumulation assay as reported by Danquah et al. (2018) [29]. Bacteria were cultured in nutrient broth with 0.4% glucose at 37°C (150 rpm) until OD_{600} reached 0.8–1.0. Cells were centrifuged (3,000 × g, 10 min), washed twice with PBS, and resuspended in PBS to OD_{600} = 0.4. Aliquots (250 µL) of bacterial suspension were transferred into Eppendorf tubes containing sub-MIC concentrations (½ MIC) of test compounds. Controls included: *Positive control*: 250 µL bacteria + 20 µg/mL verapamil. *Negative control*: 250 µL bacteria (no inhibitor). *Blank*: 250 µL PBS. Glucose (1.5 µL of 80% w/v) was added to energize efflux pumps. After pre-incubation (37°C, 10 min), 2.5 µL EtBr (50 mg/L) was added. Immediately, 250 µL aliquots were transferred to black 96-well plates. Fluorescence (λ_{ex} = 530 nm, λ_{em} = 600 nm) was measured every minute for 60 min at 37°C (BioTek Synergy H1). Relative fluorescence was plotted against time, and efflux pump inhibition was quantified by calculating the area under the curve (AUC) for fluorescence kinetics [30]. All assays were performed in triplicate with three biological replicates.

4. 4 *In vitro* cytotoxicity

The *in vitro* cytotoxicity of the synthesized compounds were assessed using Vero cells (kidney cells from African green monkey: ATCC CCL-81) following the standard MTT method [30]. The average absorbances of triplicate cells were recorded and used to determine the % Growth inhibition was determined using the formula: 100- [sample absorbance/control absorbance] x 100.

5.0 Computational methods

5.1 Protein selection and preparation

Bacterial drug targets related to bacterial folic acid biosynthesis (3TZF), bacterial multidrug exporters (2W1B), and biofilm formation (6V7X) were considered in the molecular docking studies. Inhibiting folic acid biosynthesis eventually disrupts bacterial DNA replication, stability, and integrity, while targeting multidrug exporters and biofilm-related pathways reduces bacterial resistance and enhances treatment efficacy [31]. The 3D structure of protein targets complexed with native ligands was retrieved from the Protein Data Bank (https://www.rcsb.org/). The protein structures were imported and pre-processed in Discovery Studio 2025 Client by deleting heteroatoms. Protein structures containing multiple identical chains were examined, and, for cases where the chains were structurally equivalent and each contained the active site, only one chain

was retained to eliminate redundancy and minimize computational complexity. The protein structures were energy minimized using the AMBERf4SB force field, with Gasteiger charges assigned using Antechamber in Chimera to enhance the models for molecular docking and MMGBSA calculations [32].

5.2 Ligand preparation and ADME-TOX

The 2D and 3D molecular structures of sulfamethoxazole and a curated library of 54 sulfamethoxazole derivatives were modeled and geometry-optimized using Avogadro molecular modeling software. Energy minimization was performed using the General Amber Force Field (GAFF) to refine the chemical structures and ensure accurate molecular geometries and electronic properties [33]. Partial atomic charges were assigned via the Gasteiger method, and polar hydrogens were incorporated using UCSF Chimera. The final structures were exported in Sybyl Molecular Model (MOL2) and Structure Data File (SDF) formats for subsequent computational analyses, including molecular docking simulations and scoring assessments.

Pharmacokinetic properties, such as absorption, distribution, metabolism, and excretion of the designed sulfamethoxazole derivative, were predicted from ADMETLAB 3.0 and SwissADME web servers. Toxicity parameters were assessed via Data Warrior software and ADMETLAB 3.0.

5.3 Molecular docking

Molecular docking was employed to explore the binding mechanisms of the sulfamethoxazole derivatives. A blind docking approach utilizing AutoDock Vina software was employed to generate the optimal binding poses and interactions between the modeled ligands and the prepared DHPS, AcrB, and LasR proteins [34]. In this method the grid box was programmed to encompass the entire protein structure (bind docking) without predefining any residues as critical for binding. This approach ensures that the ligand has the opportunity to interact with any portion of the protein, allowing the identification of potential binding pockets and enabling the ligand to bind to the most favorable site. The molecular docking protocol was validated by retrieving the 3D structure of the native ligand co-crystallized with *P. aeruginosa* LasR protein from the Protein Data Bank. The ligand was redocked onto the protein structure using AutoDock Vina and a blind docking approach. Five exhaustiveness values (8, 64, 128, 512, and 1064) were tested to evaluate the influence of sampling thoroughness on the redocking accuracy [35]. An improvement in accuracy was observed when increasing exhaustiveness from 8 to 64, while higher values provided no substantial additional benefit. An exhaustiveness value of 64 was selected for all subsequent docking runs. Root mean square deviation and interaction maps were assessed to ensure the

accuracy of the docking protocol. The consistency of key interactions between the redocked ligand and the protein was also checked in relation to the experimentally determined binding site. This multi-faceted validation approach ensures the reliability, reproducibility, and accuracy of the docking protocol.

5.4 Ligand efficiency

Ligand efficiency is a metric for evaluating the binding efficiencies of a ligand relative to its size [36]. Ligand efficiency was calculated using the following formula:

$$\frac{-\Delta G}{HAC}$$

Where ΔG is the binding free energy (in kcal/mol),

HAC represents heavy atom count, which is the number of non-hydrogen atoms in the ligand [37].

5.5 MM-PBSA calculations

The Molecular Mechanics Generalized Born Surface Area (MM-GBSA) method was used to estimate the binding free energy (ΔGbinding) between the protein and the optimized docked poses of each ligand. Binding free energies were calculated as the difference in free energy between the ligand–protein complex and the unbound states of the protein and ligand [38]. The binding free energy was computed according to the following relationship:

$$\Delta G_{binding} = \Delta G_{complex} - \Delta G_{ptotein} - \Delta G_{ligand}$$

$\Delta Gbinding$ is further decomposed into gas-phase interaction energy ($\Delta Ggas$) and solvation free energy (ΔGsolv). This approach enabled a robust comparison of ligand affinities and facilitated the selection of promising candidates for further analysis [39].

6.0 Results and Discussion

Integrated Computational Profiling:

6.1 *ADME-TOX*

A computational approach was used to prioritize compounds for synthesis, combining pharmacokinetic profiling with binding pose validation and free energy calculations. The initial assessment of 54 sulfamethoxazole derivatives revealed structure-property relationships about their pharmacokinetic profile.

Table 1 & 2. Predicted physicochemical, solubility and ADME properties of some of the prioritized sulfamethoxazole derivatives

Compound ID	MW (Da)	TPSA (Å²)	logS	GI absorption	PPB	BBB permeant
SMX033	252.06	72.2	-3.3378	High	92.00938	No
SMX015	296.05	98.5	-2.90194	High	92.75873	No
SMX019	315.95	72.2	-3.49824	High	94.69174	No
SMX003	283.03	115.34	-3.07732	High	85.5729	No
SMX001	283.03	115.34	-3.22374	High	95.448	No
SMX	253.05	98.22	-2.64664	High	61.27968	No

Compound ID	hERG	DILI	BSEP	Nephrotoxicity-DI	Neurotoxicity-DI
SMX033	0.075765	0.999766	0.987738	0.113391	0.034758
SMX015	0.043284	0.999995	0.916285	0.043675	0.012197
SMX019	0.042108	0.999762	0.998342	0.068108	0.042637
SMX003	0.061045	0.999999	0.749857	0.068014	0.001445
SMX001	0.035825	0.999983	0.809684	0.069278	0.006155
SMX	0.036709	0.999988	0.004074	0.071402	0.102531

Predicted properties were classified using an empirical decision scale: values between 0.0–0.3 were considered excellent, 0.3–0.7 moderate, and 0.7–1.0 poor facilitating rapid prioritization of compounds.

The derivatives were found to have favourable oral absorption potential, but aqueous solubility was a major limitation, particularly for those featuring strong electron-withdrawing groups. This property could be improved by perhydrating the isoxazole ring of the potential drug-like derivatives [40]. Positional isomerism also influenced distribution and metabolic stability. Para-substituted derivatives consistently demonstrated enhanced intestinal permeability relative to ortho or meta isomers [41]. This geometric dependence extends to plasma protein binding, where ortho-substituted derivatives exhibit elevated affinity due to restricted conformational freedom promoting hydrophobic interactions [42]. Metabolic susceptibility follows distinct electron gradients, with electron-donating groups reducing CYP450 inhibition liabilities and nitro and cyano substituents elevating risk for CYP3A4 and CYP2C19 [43]. Toxicity profiling revealed organ-specific risk stratification. Hepatotoxicity (DILI) correlated strongly with BSEP inhibition, which is linked to bile acid accumulation and mitochondrial dysfunction [44]. Cardiotoxicity risks diverged significantly, with SMX052 showing a high predicted risk of severe hERG inhibition, which is potentially fatal. Neurotoxicity and nephrotoxicity probability depend on transport

inhibition profiles, underscoring the necessity of integrated assessment of off-target effects at hepatic or renal transporters. Compound SMX012 (para-carboxylic acid) showed favourable solubility, negligible hERG inhibition, less BBB permeability, and low DILI risk, positioning it as a candidate for consideration. Trifluoromethyl derivatives were removed due to high PPB and BSEP inhibition. Furthermore, SMX016 (hepatotoxic) and SMX052 (cardiotoxic) were excluded due to intractable safety liabilities, while moderate-risk candidates such as SMX042 may require medicinal chemistry refinement to reduce CYP2C9 inhibition.

6.2 Molecular docking and ligand efficiency matrix

Molecular docking calculations were employed to identify potential DHPS inhibitors from the ADME-TOX filtered designed compounds. This docking experiment was conducted prior to investigating the effective derivatives on the LasR and AcrB protein targets. The method indicates a promising pathway for the development of new sulphonamide agents with dual mechanisms of action against bacterial cells.

The molecular docking protocol was initially validated by redocking the bound ligand N-3-oxo-dodecanosyl-homoserine lactone (OHN) and sulphonamide drug **(**08D) with LasR and DHPS, respectively, using Autodock Vina software. As expected, redocked ligands tended to have lower calculated energy values. A root mean square deviation (RMSD) of 0.20 Å was obtained for the highest OHN-ranked pose, while a value of 1.12 Å was recorded for the lowest-ranked OHN pose. The RMSD values of the sulphonamide drug (O8D) were between 0.03 and 0.67 Å. These low RMSD values (RMSD < 2 Å) suggest that the docking protocol and scoring function employed can accurately reproduce the native binding pose [45]. Furthermore, the redocked poses of the top-ranked eight complexes maintained all key interactions, implying that they were oriented in a biologically relevant manner within the binding sites, making the redocking parameters suitable for docking the designed compounds against the protein targets [46].

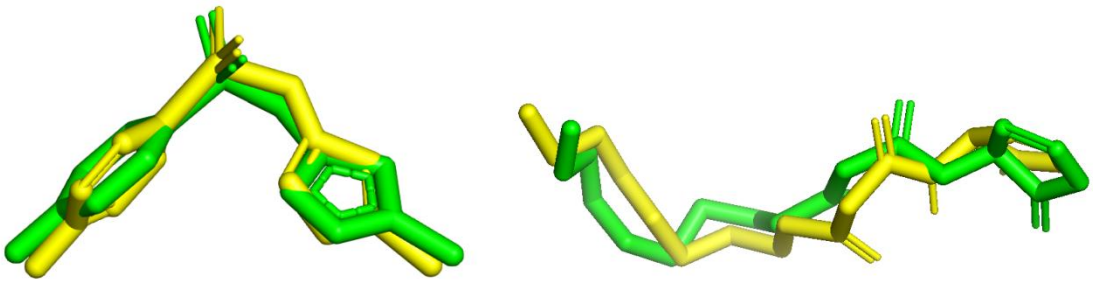

(a) (b)

Figure 2. Validation of the molecular docking protocol. (a) Superposition of the co-crystallized ligand O8D (green) with its redocked pose (yellow), yielding a root-mean-square deviation (RMSD) of 0.03 Å, indicating accurate reproduction of the experimental conformation. (b) Superposition of the co-crystallized ligand OHN (green) with its redocked pose (yellow), with an RMSD of 0.20 Å, confirming the reliability of the docking procedure.

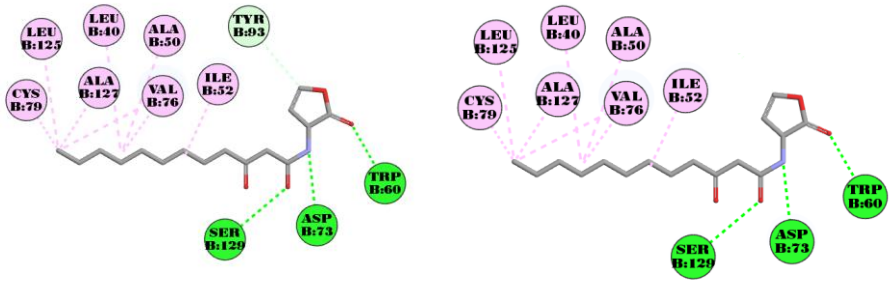

(a) (b)

Figure 3. (a) Two-dimensional interaction diagram of the co-crystallized ligand OHN in complex with 6V7X before redocking. (b) A two-dimensional interaction diagram of the same ligand after redocking, demonstrating the retention of key binding interactions within the active site.

The docking scores of the designed compounds ranged from -4.13 to -6.78 kcal/mol, with the benchmark drug, sulfamethoxazole, exhibiting a score of -4.79 kcal/mol. The results revealed a spectrum of binding affinities among the compounds, indicating potential for further investigation. The compounds were divided into four clusters based on docking score (D-score) and ligand efficiency, with more negative D-scores indicating stronger predicted binding affinities. Electron-withdrawing (EWG) substituents consistently showed stronger binding affinities than electron-donating counterparts, as the sulfonamide group served as a hydrogen bond acceptor. The most potent derivative, SMX-018, possesses a para-sulfonic acid moiety, a strong EWG, achieving a docking score of -6.78 kcal/mol. Analogues with other strong EWGs, such as carboxylic acids and trifluoromethyl groups, show moderate docking scores. Compounds functionalized with electron-donating groups exhibit moderate binding, with their docking scores clustering in a less negative range [47]. The least potent compounds are those substituted with strong para-directed EDGs, such as p-dimethylamino, p-ethoxy, and p-nitro. The ligand efficiency (L.E.) metric generally trends with the D-score, confirming that the improved binding of EWG analogues is not an artifact of increased molecular size but a more efficient interaction [48].

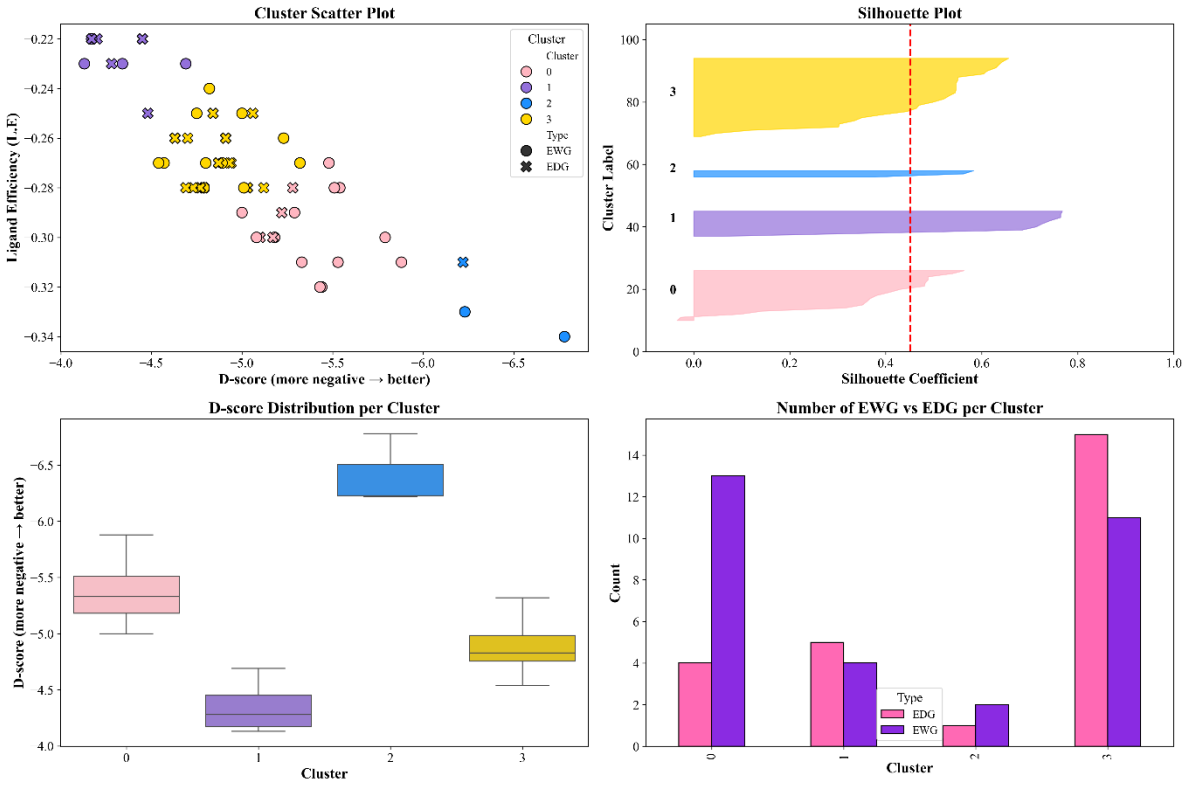

figure 4. Clustering Analysis of SulfamethoxazoleSulfamethoxazole Derivatives Based on D-score and Ligand Efficiency. *(a) Scatter plot of D-score vs. ligand efficiency colored by KMeans clusters, (b) Silhouette plot for cluster quality assessment, (c) Boxplot of D-score distribution per cluster, (d) Counts of EWG vs EDG derivatives per cluster*

Sulfamethoxazole inhibits DHPS through conserved interactions, including the electrostatic anchoring of its sulfonyl group to Lys^{221} and π-stacking of its aniline ring with Phe^{190} [49]. To address the limitations related to resistance, our structure-guided optimization procedure yielded sulfamethoxazole derivatives that created a comprehensive interaction network with the DHPS active site, as shown in Figure 1. Protein-ligand analysis identified hydrogen bonds with residues Arg^{235}, Ser^{222}, Thr^{62}, Pro^{64}, Gly189, and Lys^{221}, as well as extended hydrophobic interactions through π-stacking with Phe^{28} and Phe190, and pi-cation contacts with Lys^{221} and Arg255. The strategic recruitment of Arg^{255}, a residue essential for pterin-site recognition, may synergize with hydrogen bond interactions involving Thr^{62}, Arg^{63}, and Pro^{64} to enhance stability [50]. This binding strategy follows the substrate envelope principle by confining interactions within the native volume of p-aminobenzoic acid (PABA), thus avoiding mutation-prone regions (e.g., Phe^{33}, Leu, Pro^{69}, Thr^{67})[51]. By utilizing the phylogenetically conserved Arg^{255}, this approach connects the PABA and pterin sites, leading to a hybrid inhibitory mechanism that is less prone to single-point mutations [52].

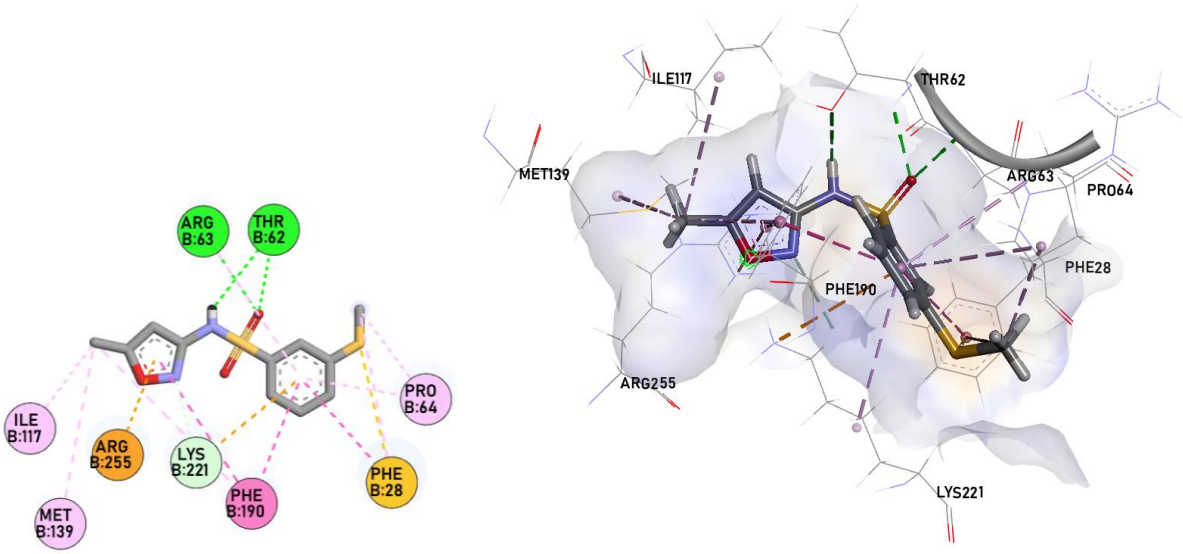

*Figure 5a. 2D and 3D interaction diagrams of the docked **SMX053** within the binding pocket of DHPS protein, showing key hydrogen bonds, hydrophobic interactions, and other non-covalent interactions with surrounding residues*

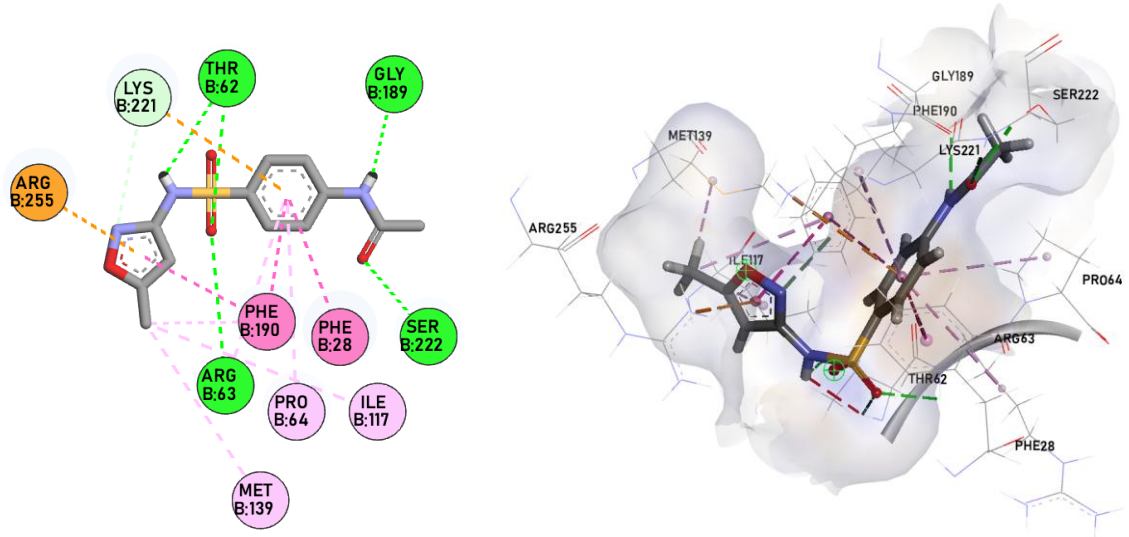

*Figure 5b. 2D and 3D interaction diagrams of the docked **SMX051** within the binding pocket of DHPS protein, showing key hydrogen bonds, hydrophobic interactions, and other non-covalent interactions with surrounding residues*

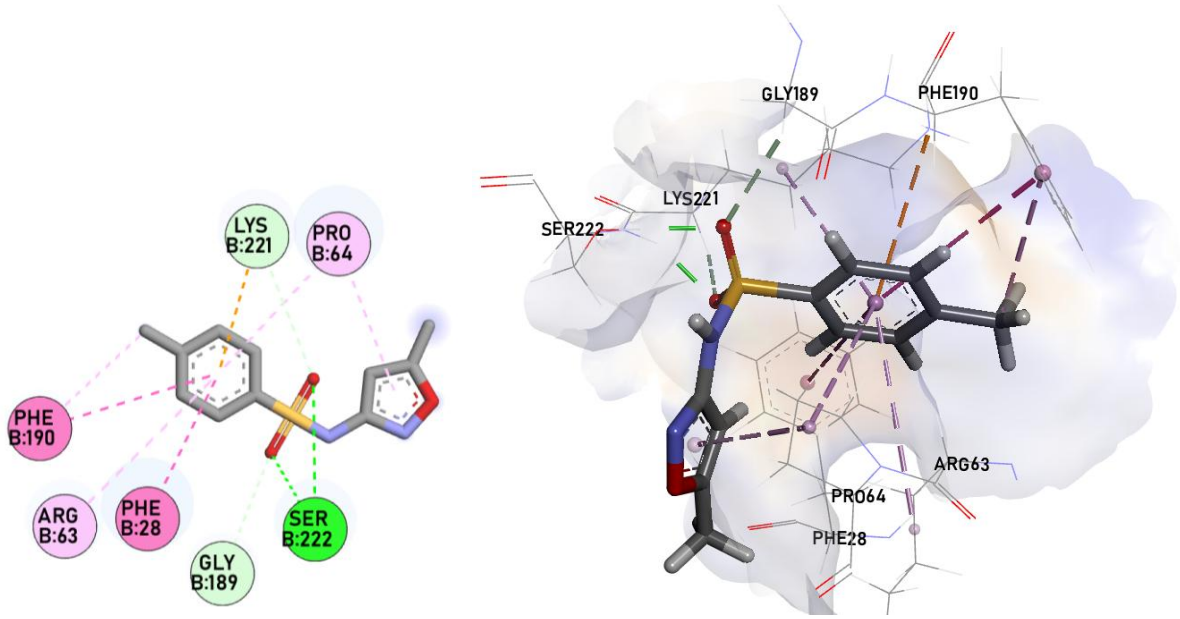

*Figure 5c. 2D and 3D interaction diagrams of the docked **SMX033** within the binding pocket of DHPS protein, showing key hydrogen bonds, hydrophobic interactions, and other non-covalent interactions with surrounding residues*

Table 3: Docking scores (D-scores) and ligand efficiencies (L.E) of sulfamethoxazole (SMX) derivatives against DHPS

compound	**Substituent (Position)**	**Type**	**Relative Strength**	D-score	L.E
SMX	p-amino	EDG	Very Strong	-4.79	-0.28
SMX001	o-nitro	EWG	Strong	-4.17	-0.22
SMX002	m-nitro	EWG	Strong	-4.75	-0.25
SMX003	p-nitro	EWG	Strong	-4.34	-0.23
SMX004	o-cyano	EWG	Strong	-4.13	-0.23
SMX005	m-cyano	EWG	Strong	-5.01	-0.28
SMX006	p-cyano	EWG	Strong	-5.53	-0.31
SMX007	o-trifluoromethyl	EWG	Strong	-5	-0.25
SMX008	m-trifluoromethyl	EWG	Strong	-5.54	-0.28
SMX009	p-trifluoromethyl	EWG	Strong	-4.69	-0.23

SMX010	o-carboxylic acid	EWG	Moderate	-6.23	-0.33
SMX011	m-carboxylic acid	EWG	Moderate	-5.79	-0.3
SMX012	p-carboxylic acid	EWG	Moderate	-5.88	-0.31
SMX013	o-methyl ester	EWG	Moderate	-5.32	-0.27
SMX014	m-methyl ester	EWG	Moderate	-5.51	-0.28
SMX015	p-methyl ester	EWG	Moderate	-4.82	-0.24
SMX016	o-sulfonic acid	EWG	Strong	-5.48	-0.27
SMX017	m-sulfonic acid	EWG	Strong	-5.23	-0.26
SMX018	p-sulfonic acid	EWG	Strong	-6.78	-0.34
SMX019	o-bromo	EWG	Weak	-5.18	-0.3
SMX020	m-bromo	EWG	Weak	-5.08	-0.3
SMX021	p-bromo	EWG	Weak	-5.44	-0.32
SMX022	o-chloro	EWG	Weak	-4.79	-0.28
SMX023	m-chloro	EWG	Weak	-5	-0.29
SMX024	p-chloro	EWG	Weak	-5.33	-0.31
SMX025	o-fluoro	EWG	Weak	-4.57	-0.27
SMX026	m-fluoro	EWG	Weak	-5.43	-0.32
SMX027	p-fluoro	EWG	Weak	-4.54	-0.27
SMX028	o-formyl	EWG	Strong	-4.8	-0.27
SMX029	m-formyl	EWG	Strong	-5.29	-0.29
SMX030	p-formyl	EWG	Strong	-4.89	-0.27
SMX031	o-methyl	EDG	Weak	-4.79	-0.28
SMX032	m-methyl	EDG	Weak	-4.73	-0.28
SMX033	p-methyl	EDG	Weak	-4.77	-0.28

SMX034	o-methoxy	EDG	Strong	-5.03	-0.28
SMX035	m-methoxy	EDG	Weak	-5.12	-0.28
SMX036	p-methoxy	EDG	Strong	-4.63	-0.26
SMX037	o-hydroxy	EDG	Strong	-5.17	-0.3
SMX038	m-hydroxy	EDG	Weak	-5.1	-0.3
SMX039	p-hydroxy	EDG	Strong	-4.69	-0.28
SMX040	o-methylamino	EDG	Strong	-4.87	-0.27
SMX041	m-methylamino	EDG	Weak	-4.7	-0.26
SMX042	p-methylamino	EDG	Strong	-5.22	-0.29
SMX043	o-dimethylamino	EDG	Very Strong	-4.91	-0.26
SMX044	m-dimethylamino	EDG	Weak	-4.84	-0.25
SMX045	p-dimethylamino	EDG	Very Strong	-4.2	-0.22
SMX046	o-ethoxy	EDG	Strong	-4.17	-0.22
SMX047	m-ethoxy	EDG	Weak	-5.28	-0.28
SMX048	p-ethoxy	EDG	Strong	-4.28	-0.23
SMX049	o-acetamido	EDG	Moderate	-5.06	-0.25
SMX050	m-acetamido	EDG	Moderate	-6.22	-0.31
SMX051	p-acetamido	EDG	Moderate	-4.45	-0.22
SMX052	o-methylthio	EDG	Moderate	-4.93	-0.27
SMX053	m-methylthio	EDG	Moderate	-4.94	-0.27
SMX054	p-methylthio	EDG	Moderate	-4.48	-0.25

MMGBSA is a computationally efficient method that combines molecular mechanics energies for both protein and ligand atoms with solvation terms derived from the Generalized Born model [53]. In the current study, MM-GBSA calculations were mainly carried out with the aim of ligand conformation refinement and ranking ligands according to their affinity against a particular protein

target, and not with the purpose of directly comparing binding affinities between different proteins.

This approach served as an additional selection criterion to advance the designed compounds to the next stage. Following MMGBSA refinement in the PRIME module, twenty-four (24) derivatives progressed to the next phase of computational profiling. These derivatives mainly exhibited superior MM-GBSA binding energies against DHPS compared to sulfamethoxazole (SMX: -45.03 kcal/mol), thereby confirming the effectiveness of substitution strategies across various chemical classes for the specified target. High-affinity compounds included derivatives featuring electron donating groups (e.g., SMX051: -58.46 kcal/mol), electron-withdrawing groups (e.g., SMX018: -49.62, SMX023: -49.35, SMX033: -47.86 kcal/mol), and polar functionalities (e.g., SMX050: -49.68 kcal/mol).

Table 4: Energy Decomposition Analysis of SMX Derivatives against DHPS

Derivative	**Bind**	**Coulomb**	**Covalent**	**Hbond**	**Lipo**	**Packing**	**Solv_GB**	**vdW**
SMX	-45.03	-21.71	3.26	-2.95	-9.82	-3.98	24.36	-34.18
SMX005	-46.93	-19.81	2.28	-1.09	-9.72	-1.23	19.48	-36.82
SMX010	-47.24	-35.96	3.31	-2.07	-9.15	-0.94	29.28	-31.71
SMX012	-47.66	-28.35	2.82	-2.74	-9.79	-2.33	26.67	-33.94
SMX015	-45.86	-15.39	2.53	-2.16	-10.76	-2.44	21.86	-39.49
SMX017	-46.96	-26.88	3.85	-1.54	-8.76	-1.11	24.52	-37.03
SMX018	-49.62	-25.01	2.57	-2.62	-8.73	-2.75	21.79	-34.86
SMX020	-46.24	-21.66	2.97	-2.15	-10.82	-1.99	21.78	-34.38
SMX023	-49.35	-27.66	3.01	-2.17	-12.92	-3.92	30.58	-36.28
SMX024	-46.12	-21.79	2.98	-2.47	-13.07	-4.14	25.75	-33.39
SMX026	-45.54	-27.88	3	-2.18	-11.57	-3.95	30.83	-33.77
SMX029	-49.17	-31.5	3.99	-2.89	-10.15	-3.88	33.52	-38.25
SMX030	-47.51	-32.69	3.33	-2.68	-10.25	-4.12	33.39	-34.48
SMX032	-47.01	-20.31	3.03	-2.19	-13.09	-3.93	25.26	-35.78
SMX033	-47.86	-9.19	0.12	-1.43	-12.61	-1.41	11.55	-34.89
SMX035	-45.45	-21.53	2.75	-2.24	-12.87	-3.97	29.83	-37.41
SMX037	-45.46	-24.98	0.31	-1.34	-8.85	-0.89	19.21	-28.92
SMX038	-46.21	-25.92	3.25	-2.32	-11.62	-4.02	28.28	-33.86

SMX041	-48.43	-22.47	3.46	-2.28	-12.99	-4.01	27.05	-37.18
SMX042	-46.89	-21.07	3.21	-2.94	-10.85	-3.99	25.82	-37.07
SMX044	-45.53	-10.35	0.95	-1.46	-12.85	-0.97	14.37	-35.21
SMX047	-49.28	-18.47	3.73	-2.16	-12.75	-2.06	22.54	-40.11
SMX050	-49.68	-32.27	7.06	-3.11	-11.44	-3.97	35.22	-41.16
SMX051	-58.46	-43.82	5.1	-3.58	-11.15	-3.97	40.32	-41.36
SMX053	-50.59	-26.91	5.73	-2.12	-13.11	-3.89	30.82	-41.1

The differences in the MMGBSA binding free energy between sulfamethoxazole and the filtered derivatives indicated that the derivatives fit better into the DHPS binding pockets or adjacent binding clefts. This improved fit creates strong polar and nonpolar contacts with the active site residues, effectively holding the derivatives within the binding site or in allosteric clefts [54]. The successful candidates exhibited high positive solvation energy values, implying a desolvation penalty upon binding; however, this penalty was outweighed by the strong van der Waals interactions and Coulombic energies. The performance of the top binders was attributed to their Coulombic energy and favourable van der Waals forces, which are significantly more advantageous than those of sulfamethoxazole. This evidence suggests that the successful derivatives enhance the formation of stronger salt bridges, dipole-dipole interactions, or charge-assisted hydrogen bonds and van der Waals contact with the DHPS active site. It also implies that modifications improving electrostatic fit without compromising van der Waals contacts are likely to achieve better binding to the DHPS protein target [55]. The free binding energies from the simulation further confirmed the strength of ligand binding to the target and their favorable interactions with DHPS, as evidenced by the docking studies.

Derivatives that exhibited superior MMGBSA scores compared to sulfamethoxazole were selected for molecular docking and MMGBSA calculations with the LasR and AcrB proteins as distinct targets, where the ranking of derivatives by MM-GBSA was assessed only in the framework of the distinct target. In the context of quorum-sensing inhibition, the top 24 DHPS-targeting derivatives were evaluated against *Pseudomonas aeruginosa* LasR. While sulfamethoxazole (SMX) demonstrated an MMGBSA score of -43.30 kcal/mol, 17 derivatives displayed enhanced binding free energies (dBind), particularly SMX018 (-52.81 kcal/mol) and SMX047 (-51.10 kcal/mol). Docking analysis indicated competitive displacement of the autoinducer 3-oxo-C12-HSL through hydrogen bonding with residues including Thr115, Ser129, Thr75, Tyr56, Leu39, and Gly38. Additional interactions included π-π stacking with Tyr64, pi-sulfur interactions with Asp73, and hydrophobic

interactions with Val76, Leu125, Ala127, Leu40, Leu36, and Ala50 as illustrated in figure 6a-6c.

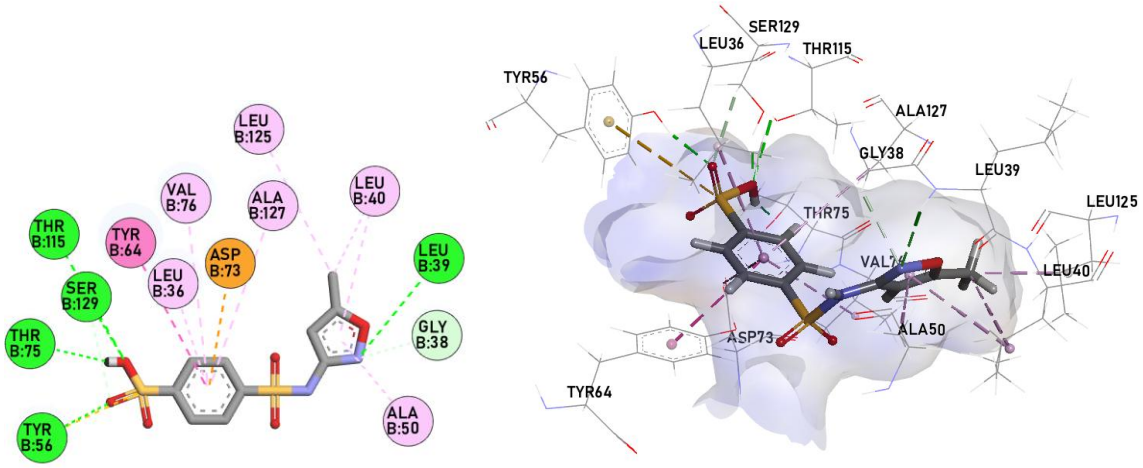

*Figure 6a. 2D and 3D interaction diagrams of the docked **SMX018** within the binding pocket of LasR (PDB ID: 6v7x) protein, showing key hydrogen bonds, hydrophobic interactions, and other non-covalent interactions with surrounding residues*

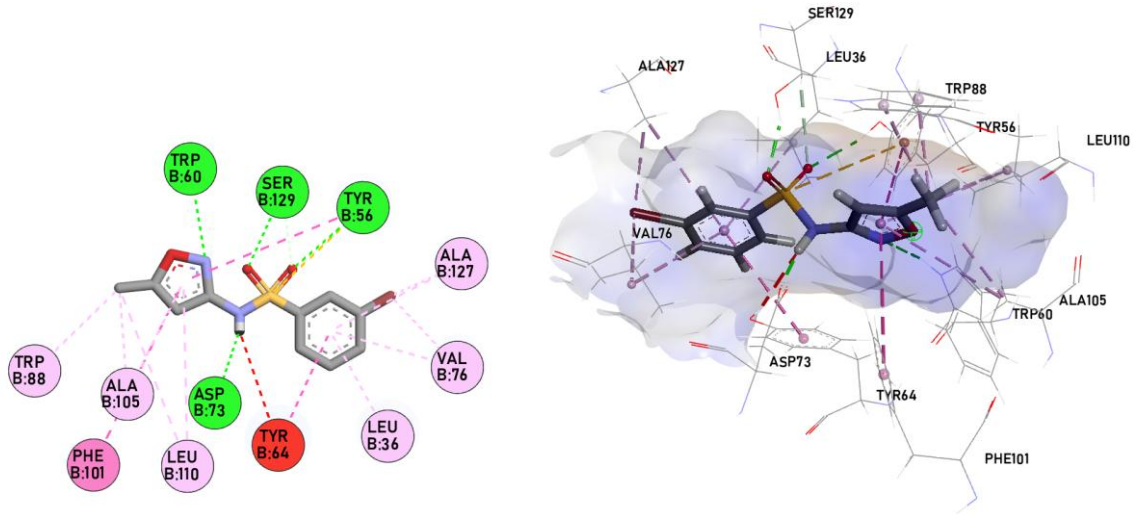

*Figure 6b. 2D and 3D interaction diagrams of the docked **SMX020** within the binding pocket of LasR (PDB ID: 6v7x) protein, showing key hydrogen bonds, hydrophobic interactions, and other non-covalent interactions with surrounding residues.*

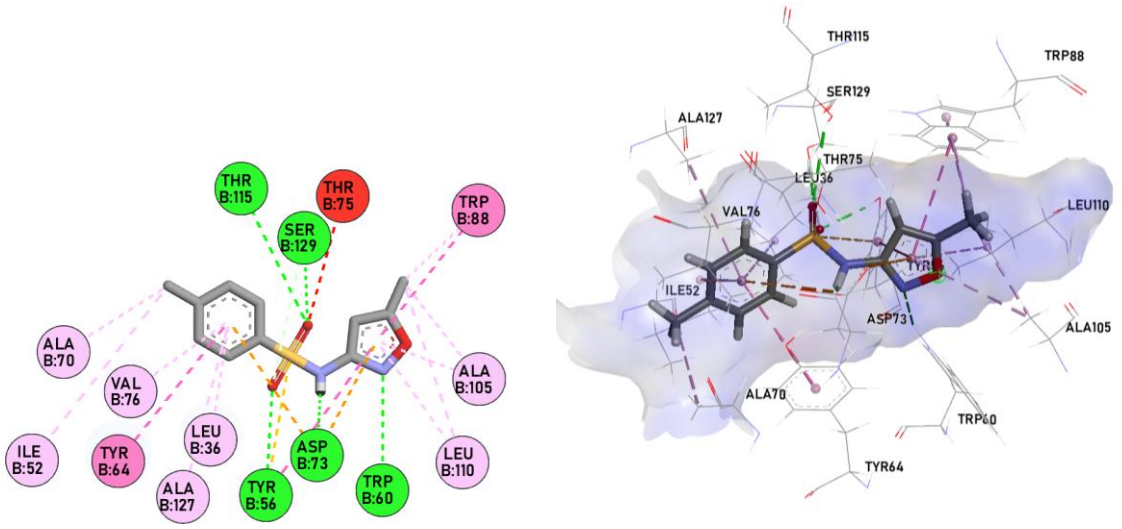

Figure 6c. 2D and 3D interaction diagrams of the docked ***SMX033*** *within the binding pocket of LasR (PDB ID: 6v7x) protein, showing key hydrogen bonds, hydrophobic interactions, and other non-covalent interactions with surrounding residues.*

Moreover, these derivatives caused allosteric disruption by occupying the Ile^{52}-Ala^{50} hydrophobic subpocket, which impaired dimerization and DNA binding, resembling the mechanism of phage protein Aqs1 [56]. The incorporation of halogen atoms in compounds such as SMX019 and SMX020 enhanced potency via halogen bonding (e.g., with Val76) and hydrophobic filling of subpockets. Structure-activity relationships of the LasR complex suggested that optimal hydrophobic rings were essential for acyl pocket occupation, with increased rigidity leading to reduced entropic penalties and improved hydrogen bonding with the sulphonamide functional group[57]. Biologically, these derivatives can disrupt the LasR-RhlR-PQS hierarchy, thereby inhibiting virulence factors such as elastase and pyocyanin.

For efflux pump inhibition, the same set of compounds was assessed independently against *E. coli* AcrB. The binding free energies observed differ from the values obtained when performing free binding energy calculations of the compounds against DHPS and LasR independently. In this regard, SMX exhibited a free binding energy of -34.17 kcal/mol, while 7 derivatives showed improved affinity. The derivatives target the periplasmic vestibule in AcrB, engaging Phe664 and Pro669, which are critical for van der Waals interactions with native substrates such as deoxycholate, ciprofloxacin, and ethidium. Notably, deoxycholate binds in the same vestibule region and forms a hydrogen bond with Ser715, in addition to hydrophobic interactions with Phe664 [58], supporting the biological relevance of this site. Novel interactions include hydrogen bonds with Arg^{717} (unused by ciprofloxacin/ethidium), creating a steric block at the vestibule entrance [1, 4]. Pi-sulfur bonds with Met^{575} and hydrogen bonds with Pro718, Gly720, Asn719, Ala665, Asn667, Met649, Thr648, Thr678, and Gln^{830} further enhance entropy to counter

vestibule flexibility [58].

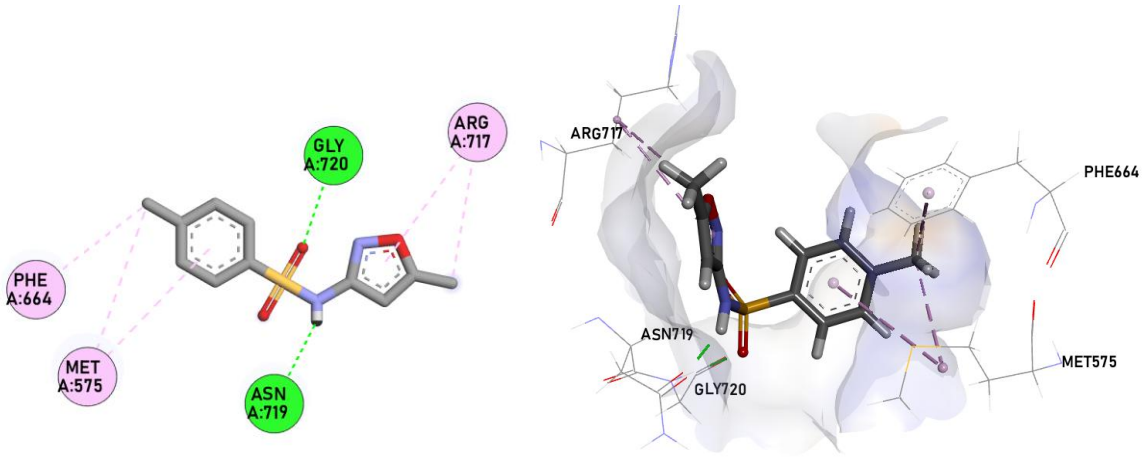

Figure 7a. 2D and 3D interaction diagrams of the docked ***SMX033*** *within the binding pocket of AcrB (PDB ID: 2w1b) protein, showing key hydrogen bonds, hydrophobic interactions, and other non-covalent interactions with surrounding residues.*

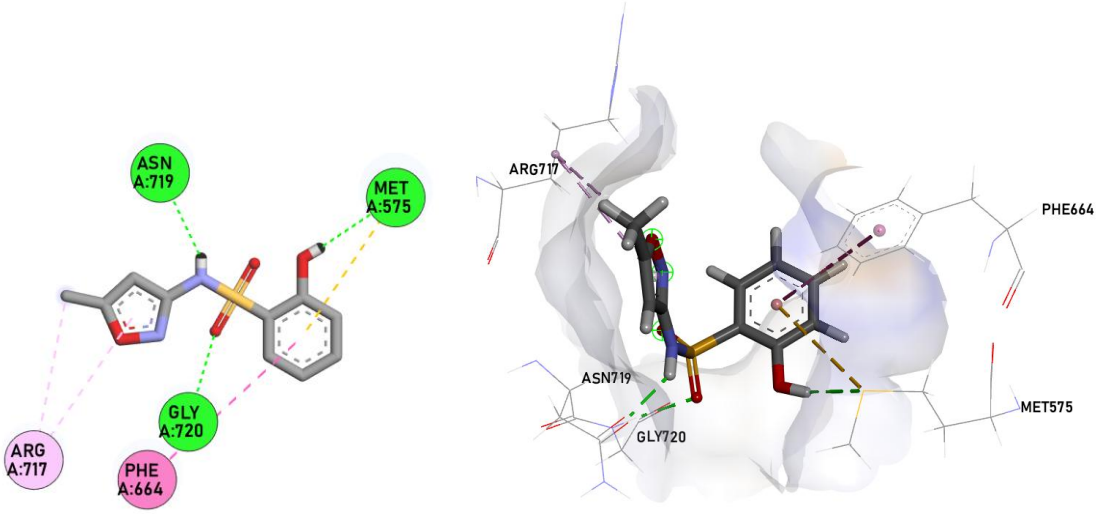

Figure 7b. 2D and 3D interaction diagrams of the docked ***SMX037*** *within the binding pocket of AcrB (PDB ID: 2w1b) protein, showing key hydrogen bonds, hydrophobic interactions, and other non-covalent interactions with surrounding residues.*

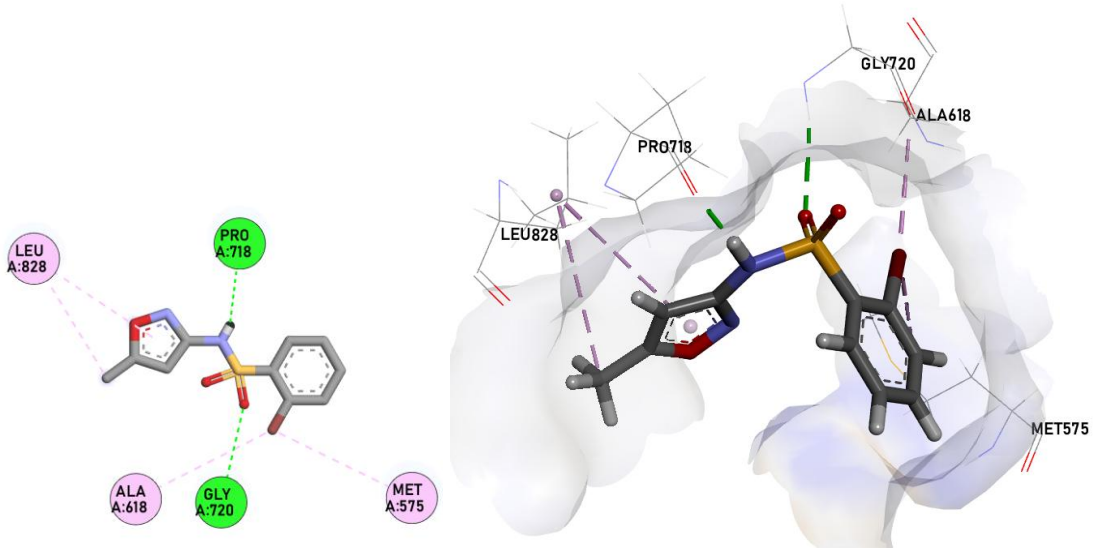

Figure 7c. 2D and 3D interaction diagrams of the docked ***SMX019*** *within the binding pocket of AcrB (PDB ID: 2w1b) protein, showing key hydrogen bonds, hydrophobic interactions, and other non-covalent interactions with surrounding residues.*

Mechanistically, vestibule confinement arrests AcrB in the "loose" (L) state, as was observed in the deoxycholate-bound AcrB structure, preventing rotational transition to export-competent conformations ("tight"/"open" states) necessary for efflux pumping.

On the basis of the results of docking interactions and ADME/toxicity predictions obtained using the integrated MM-GBSA scores, five derivatives (SMX001, SMX003, SMX015, SMX019, and SMX033) were prioritized for synthesis and biological evaluation. This selection was designed to rigorously validate our computational predictions and probe critical structure-activity relationships. Specifically, SMX001 and SMX003 tested the hypothesis that electron-withdrawing groups enhance binding affinity to DHPS. SMX015 was chosen to evaluate whether incorporating polar functionality enabled high-affinity dual engagement with both DHPS and LasR targets. To probe the predicted role of halogen bonding in LasR inhibition, SMX019 was selected. Finally, SMX033 served as a critical benchmark for ADME/toxicity, boasting a favorable predicted solubility and safety profile, in addition to its strong van der Waals contacts within AcrB's hydrophobic vestibule.

6.3 Design strategy and chemistry of the sulfamethoxazole derivatives.

A small library of five sulfamethoxazole derivatives was synthesized by a pH-dependent reaction between 3-amino-5-methylisoxazole and sulphonyl chlorides 30 (Figure 1). The progress of the reaction was monitored using aluminum-coated backing silica gel TLC plates. After purification by silica column chromatography with a mobile phase of CH_2Cl_2 (dichloromethane): Et_2O (diethyl ether) [60:40], all corresponding sulfamethoxazole derivatives were obtained in 65-78%

yields (Figure 2, Table 4.1).

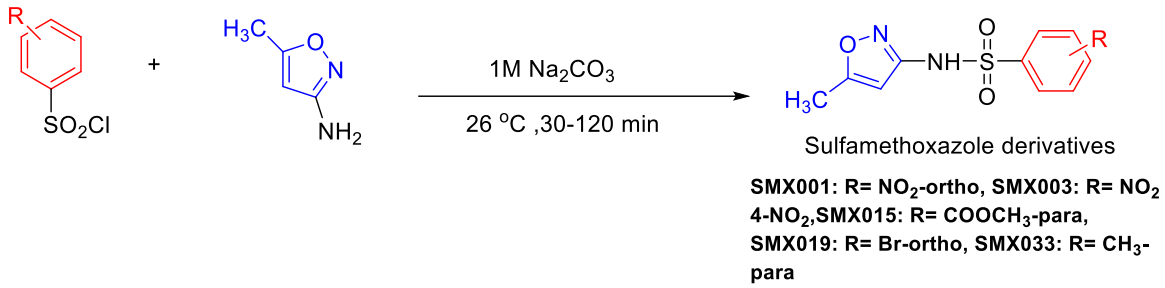

Figure 8: Scheme for the synthesis of the substituted sulfamethoxazole.

The compounds were confirmed by their structures using ^{1}H NMR, ^{13}C NMR spectroscopy and HRMS. The ^{1}H NMR spectrum of compound SMX033 showed a broad peak between 6.24 and 6.26 ppm, indicating the formation of the sulfonamide group. The doublet peaks observed downfield at 7.68 to 7.70 ppm correspond to the p-disubstituted sulfonyl aromatic portion. The HRMS analysis revealed the molecular ion peak calculated for $[M + H]^{+}$ as 252.0569, while the observed peak was 253.0649. Based on the structural evaluation, compound SMX033 was designated as 4-methyl-N-(5-methylisoxazol-3-yl)benzenesulfonamide. The primary amino group of sulfamethoxazole was converted through synthesis to generate compounds with electron-withdrawing and donating groups on the benzene sulfonyl portion, which were synthesized in good to excellent yields (60–78%).

Table 5: Physicochemical characterisation data of the synthesised compounds

Compound	-R	Molecular formula	Calculated molecular weight	Melting point (°C)	Yield (%)
SMX001	*o*-NO_2	$C_{10}H_9N_3O_5S$	283.03	116-118	78
SMX003	*p*-NO_2	$C_{10}H_9N_3O_5S$	283.03	118-120	71
SMX015	*p*-$COOCH_3$	$C_{11}H_{12}N_2O_3S$	296.06	126-129	75
SMX019	*o*-Br	$C_{10}H_9BrN_2O_3S$	315.95	164-167	75
SMX033	*p*-CH_3	$C_{11}H_{12}N_2O_3S$	252.06	125-127	65

Table 6: MIC of susceptible organisms and cytotoxicity comparison data of the synthesised compounds

Compound	-R	Molecular formula	[a]MIC (μg/mL) ± SEM	[b]CC_{50} (μM) ± SEM
SMX001	*o*-NO_2	$C_{10}H_9N_3O_5S$	441.00 ± 0.050	112.22 ± 0.060
SMX003	*p*-NO_2	$C_{10}H_9N_3O_5S$	441.00 ± 0.002	125 ± 0.060
SMX015	*p*-$COOCH_3$	$C_{11}H_{12}N_2O_3S$	61.98 ± 0.060	186.00 ± 0.005
SMX019	*o*-Br	$C_{10}H_9BrN_2O_3S$	395.63 ± 0.025	121.10 ± 0.060
SMX033	*p*-CH_3	$C_{11}H_{12}N_2O_3S$	61.98 ± 0.020	286.20 ± 0.001
Ciprofloxacin	-	$C_{17}H_{18}FN_3O_3$	3.91 ± 0.0001	No inhibition

[a] MIC: Minimum inhibitory concentration of compounds SMX015 and SMX033 demonstrating highest inhibitory activity against *P. mirabilis*, *S. typhi*, and *E. coli* (MIC: 15.625 μg/mL). [b] CC_{50} =50 % cytotoxic concentration on Vero cells [c] SI =Selective index (CC_{50}/MIC); [d] % inhibition during preliminary screening; Ciprofloxacin positive control. [a] IC_{50} and [b] CC_{50} values represent triplicate determinations (three determinations from three different experiments). Nd: no visible and significant inhibition hence SI determination not available.

6.4 Biological evaluation

6.4.1 *Minimum inhibitory concentration (MIC) and cytotoxicity*

The MICs of the synthesized compounds against test organisms (*Proteus mirabilis, Salmonella typhi, Escherichia coli, and Pseudomonas aeruginosa*) were determined using the broth microdilution technique. Figure 9 shows the MIC values of the compounds within the range of 15.625 to 125 μg/mL. All the synthesized derivatives exhibited MIC values < 100 μg/mL against the test organisms, except *Pseudomonas aeruginosa*, which showed MIC values > 100 μg/mL for SMX001, SMX003, and SMX019. The cytotoxicity data on the compounds is shown in Table 6

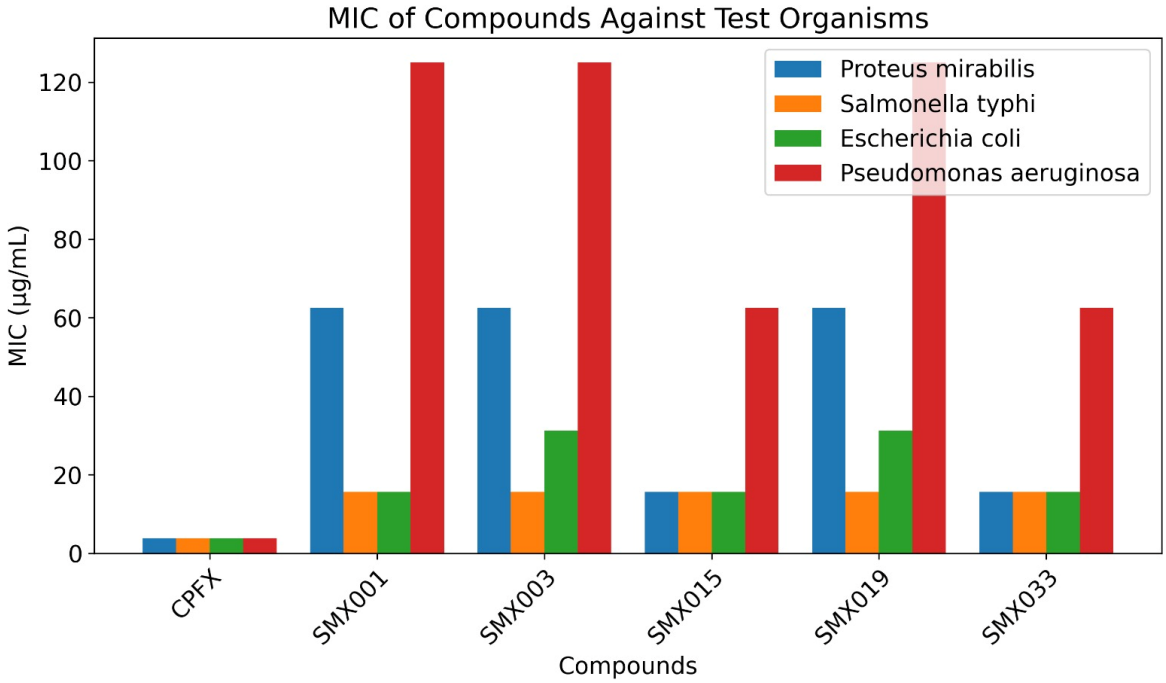

Figure 9: Minimum Inhibitory Concentrations (MICs) of SMX Derivatives against ESKAPE Pathogens

The *in vitro* antibiotic potential of the five (5) sulfamethoxazole derivatives was assessed individually using the high-throughput spotting assay method. The MIC of the five (5) synthesized compounds was determined alongside ciprofloxacin and DMSO as positive and negative controls, respectively. All compounds showed significant antibacterial activity against *P. mirabilis*, *S. typhi*, and *E. coli* (MICs 15.625-62.5 µg/mL), although they were less potent than ciprofloxacin (3.91 µg/mL). Compounds SMX015 and SMX033 demonstrated high inhibitory activity against *P. mirabilis*, *S. typhi*, and *E. coli* (MIC: 15.625 µg/mL). Compounds SMX001, SMX003, and SMX019 recorded inhibitory activity against *S.* typhi (MIC: 15.625 µg/mL). Additionally, compound SMX001 also recorded inhibitory activity (MIC: 15.625) against *E. coli*. Activity against the more resistant *Pseudomonas aeruginosa* was markedly reduced (MICs 62.5-125 µg/mL) compared to ciprofloxacin (3.91 µg/mL), indicating substantial intrinsic resistance. Compound SMX033 features a methyl group at the *para* position, whilst compounds SMX015 and SMX001 feature *p*-methyl ester and o-nitro groups, respectively. SMX033 demonstrated comparable or improved activity relative to sulfamethoxazole against most tested Gram-negative pathogens. Compound SMX033 consistently demonstrated significant antibacterial activity against all tested pathogens, suggesting its potential as a broad-spectrum agent. *Pseudomonas aeruginosa*, the most resistant pathogen, was susceptible to SMX033 and SMX019 at 62.5 µg/mL and SMX001, SMX003, and SMX015 MIC at 125 µg/mL, indicating moderate inhibition. The observed MIC values (15.625 - 125 µg/mL) against Gram-negative pathogens align with the computational ranking based on

MMGBSA binding free energies. Notably, SMX033 (*p*-CH_3) and SMX015 (*p*-$COOCH_3$) consistently exhibited the lowest MICs (most potent activity), particularly against *P. mirabilis*, *S. typhi*, and *E. coli* (15.625 μg/mL). Their strong computational scores directly support this strong inhibitory activity. SMX033 demonstrated exceptional MMGBSA scores against all three targets: DHPS (dBind: -47.86 kcal/mol), LasR (dBind: -48.92 kcal/mol), and AcrB (dBind: -41.15 kcal/mol). Its high affinity, predicted to stem from optimal van der Waals contacts in the hydrophobic vestibules of AcrB and LasR, translates to effective bacterial growth inhibition by simultaneously disrupting folate synthesis, quorum sensing, and efflux. **SMX015** also showed strong multi-target binding potential *in silico*, with favorable energies against DHPS (dBind: -45.86 kcal/mol) and LasR. Its polar ester group was predicted to facilitate dual engagement, which is consistent with its potent and broad-spectrum MIC results [59]. The reduced activity against *P. aeruginosa* (MICs: 62.5–125 μg/mL) for all compounds was anticipated. This pathogen possesses a notoriously impermeable outer membrane and highly efficient efflux systems, which our *in silico* models, focused on target binding, would not fully account for. *P. aeruginosa* is highly resistant and could require different derivatives or scaffolds [60]. However, the fact that **SMX033** and **SMX015** still showed the best activity (MIC = 62.5 μg/mL) against this resilient pathogen underscores the strength of the multi-target approach, as overcoming its defense likely requires potent inhibition of multiple resistance pathways simultaneously [61]. Compound SMX 033 is arguably the most potent when compared with ciprofloxacin because the substitution of the methyl in the phenyl ring present at the *para* position of the isoxazole nucleus enhanced the antimicrobial activity and decreased the cytotoxic activity of compound SMX 033. Compound SMX 033 exhibited reduced cytotoxicity against Vero cell lines, with a CCC_{50} value of 286.20 μM suggesting its high selectivity towards the pathogens

6.4.2 *Biofilm Formation Inhibition*

Biofilms are structured communities of microorganisms embedded in an extracellular matrix, offering protection against antimicrobials [62]. The ability to inhibit biofilm formation is critical for treating chronic infections, as biofilms are notoriously resistant to conventional antibiotics. By preventing biofilm development, the compounds could reduce microbial persistence and improve treatment outcomes. Biofilm inhibition might result from interference with adhesion, quorum sensing, or EPS synthesis [62,63,64]. Biofilm formation inhibition effects of the compounds SMX033, SMX019, SMX003, SMX015, and SMX001 at sub-MIC concentrations against *Proteus mirabilis, Salmonella typhi, Escherichia coli, and Pseudomonas aeruginosa* were analysed and represented as a percentage of inhibition in Figure 1 and Figure 2. The antibiotic's subminimal inhibitory

concentration (sub-MIC) can influence the biofilm formation capacity of bacterial pathogens, thereby impacting the pathogenesis and infection outcomes [65]. The compounds exhibited excellent biofilm inhibition. All derivatives, particularly SMX033, SMX015, and SMX001, achieved exceptional inhibition (>98.5%) against the tested organisms, significantly outperforming the parent drug ciprofloxacin (94.35). This result directly correlates with the molecular docking predictions. Our models indicated that these derivatives competitively displace the native autoinducer (OHN) in the LasR binding pocket by forming key hydrogen bonds with residues Thr75, Tyr56, and Ser129. Furthermore, they were predicted to cause allosteric disruption by occupying the critical Ile^{52}-Ala^{50} hydrophobic subpocket, impairing LasR dimerization and DNA binding, a mechanism known to inhibit biofilm formation profoundly [66]. The superior experimental biofilm inhibition of SMX019 (o-Br) against *E. coli* aligns with its *in silico* prediction of enhanced potency through halogen bonding (e.g., with Val76 in LasR). The strong experimental biofilm inhibition across the board confirms the computational prediction that targeting LasR is a viable and effective strategy for these sulfamethoxazole derivatives.

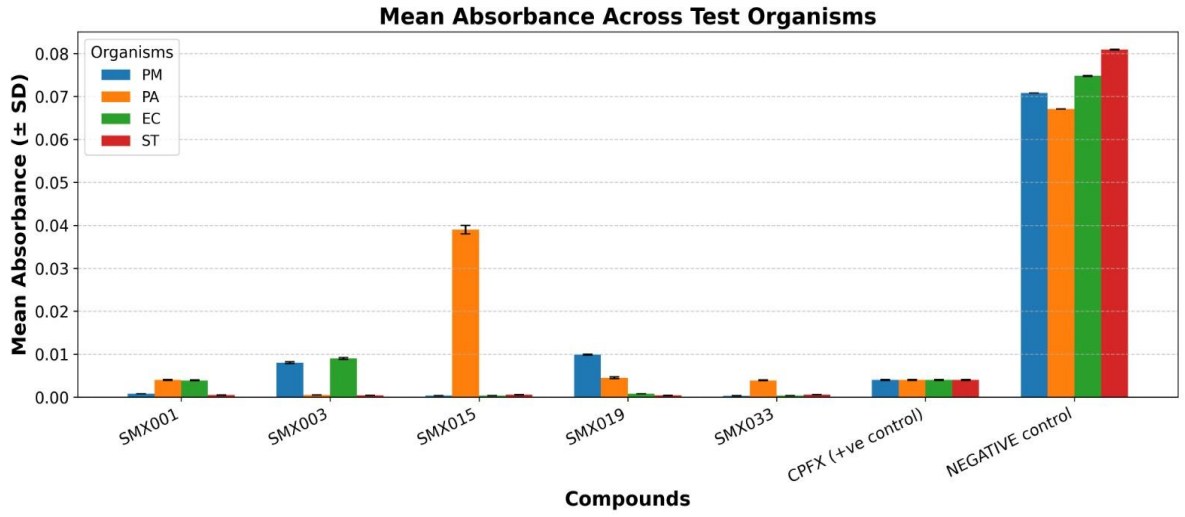

Figure 10a. Mean absorbance of SMX derivatives

Absorbance reflects remaining biofilm biomass, where lower values indicate greater inhibition [67]. Each value is the average of replicate readings for three determinations with their standard deviation (SD). The negative control, which contained no antimicrobial treatment, served as a baseline for maximum biofilm formation in the organism.

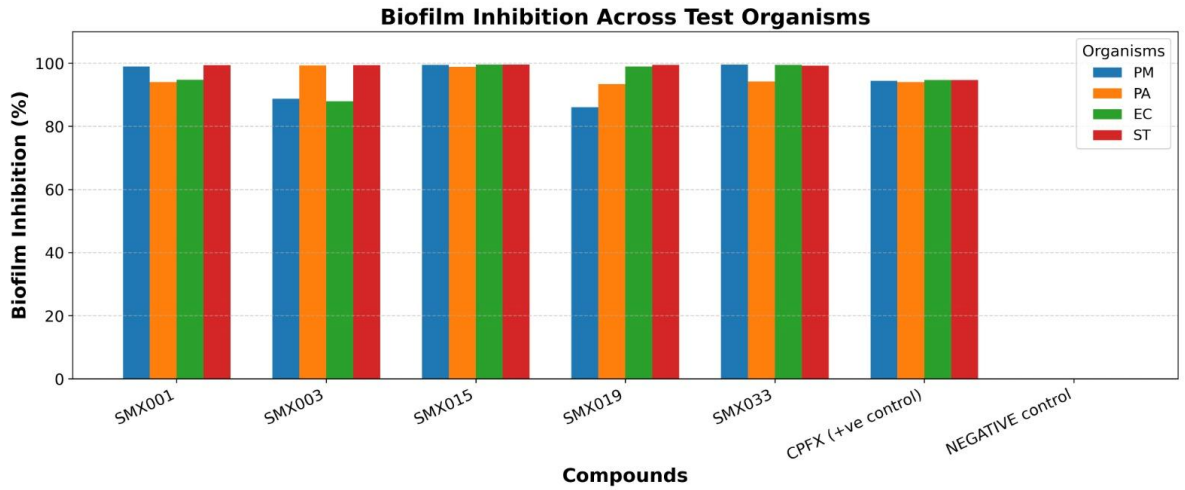

Figure 10b. Biofilm inhibition of derivatives against test organisms. All derivatives achieved exceptional biofilm inhibition (>99%) against Salmonella typhi compared to ciprofloxacin (94.35%); compounds SMX033, SMX015, and SMX001 demonstrated excellent biofilm inhibition (>98.5%) against Proteus mirabilis; and SMX033, SMX015, and SMX019 also showed excellent biofilm inhibition (>98%) against, Escherichia coli. Compared to ciprofloxacin, the derivatives performed significantly.

6.4.3 *Ethidium Bromide Efflux Pump Inhibition Assay*

Efflux pumps are membrane proteins found in bacteria that actively expel toxic substances including antibiotics out of the pathogen cell [68]. Some of these efflux pumps are non-specific, removing a wide range of drug molecules, while others are selective. Efflux pump inhibitors are compounds that block the activity of these pumps, thereby increasing the intracellular concentration of antibiotics and restoring their effectiveness [69]. The relevance of efflux pump inhibition still remains intact as it aids in combating antibiotic resistance. Overexpression of efflux pumps is a common mechanism of multidrug resistance, especially in pathogens like *Pseudomonas aeruginosa*, *Escherichia coli,* and *Acinetobacter baumannii* [70]. Efflux pump inhibitors (EPIs) enhance drug potency by retaining antibiotics inside bacteria cells, thereby lowering the required dose of antibiotic and reducing side effects. Combining an antibiotic (even older and less tolerated drugs) with EPIs can offer a synergistic effect [71, 72]. Ethidium bromide was utilized in the evaluation of the efflux pump inhibition potential of the compounds. Because it may intercalate DNA, which breaks down DNA structure and causes cell death, the dye ethidium bromide (EB) possesses antibiotic activity [73]. The efflux pump is the sole defense mechanism that bacteria use to fend off the effects of ethidium bromide [74]. This method has been used in many studies to investigate the presence or absence of efflux pumps in combination with traditional efflux pump inhibitors [75, 76]. To evaluate the compound's effectiveness, the efflux pump inhibition experiment used ethidium bromide (EtBr) as a substrate. The premise of this experiment is that EtBr has strong

intracellular fluorescence. As it keeps building up, it binds to DNA and creates a growing fluorescence. When they build up inside the bacterial cells, the fluorescence intensity rises, indicating that the efflux pump mechanism is being inhibited. A low fluorescence measurement occurs when the cell pumps out EtBr in the absence of efflux pump inhibitory action. The fluorescence intensity was recorded at an interval of everyone (1) minute for a total period of sixty (60) minutes. Compound SMX033 (CH3-para) demonstrated a remarkable inhibition of the efflux pump and was the strongest EPI overall.

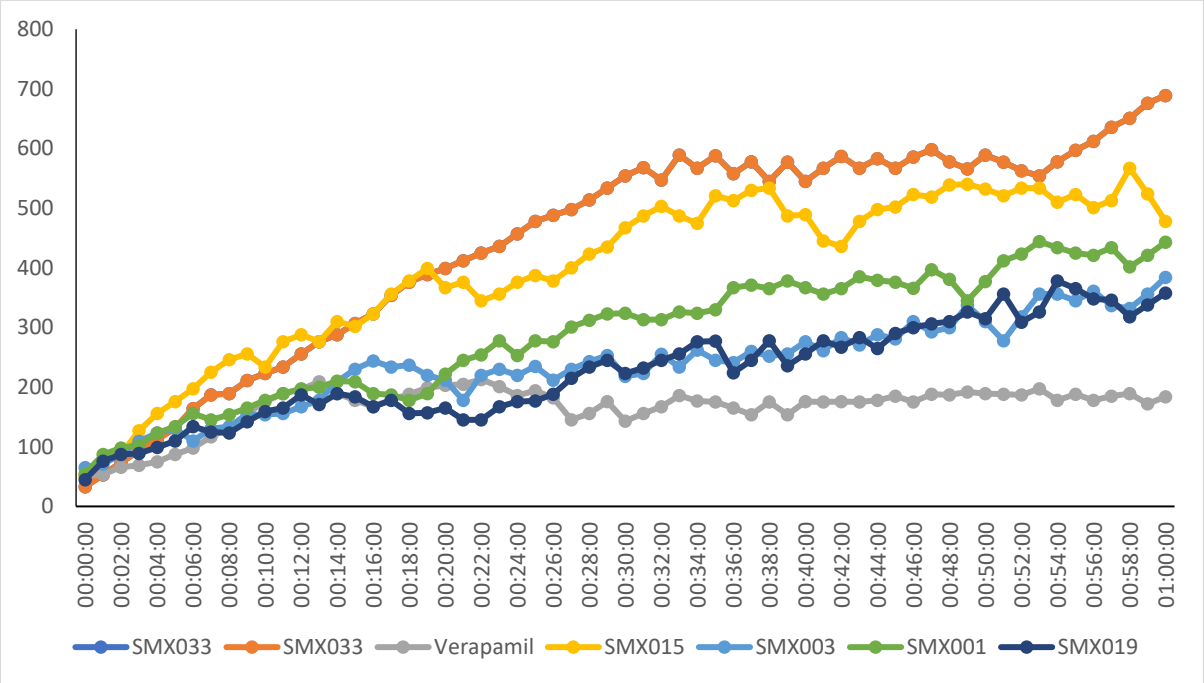

Figure 11a. Time-dependent efflux pump inhibition in Escherichia coli by verapamil and sulfamethoxazole derivatives.

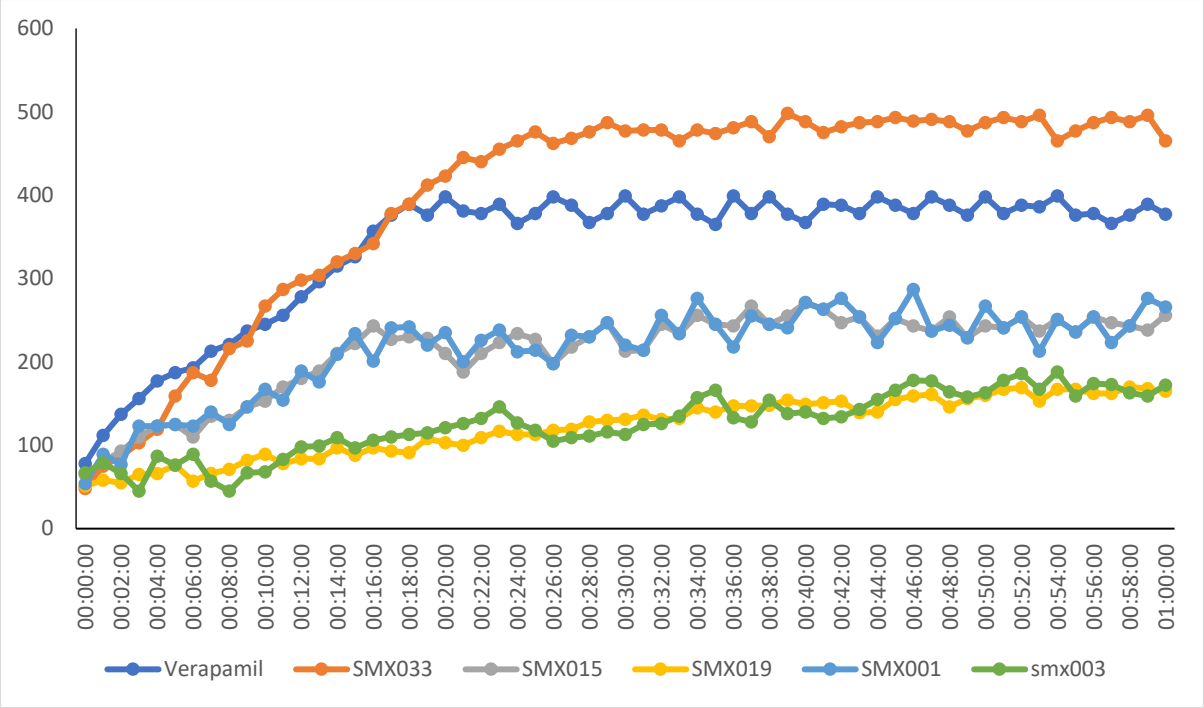

Figure 11b. Time-dependent efflux pump inhibition in Pseudomonas aeruginosa by verapamil and sulfamethoxazole derivatives.

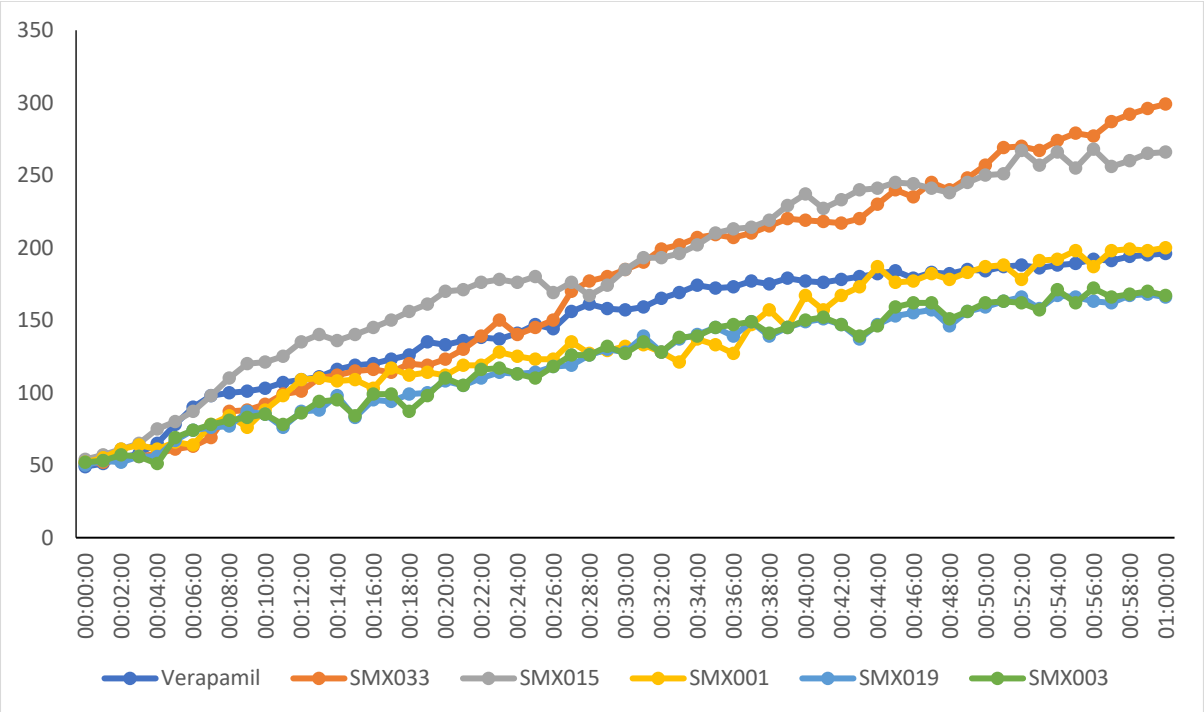

Figure 11c. Time-dependent efflux pump inhibition in Proteus mirabilis by verapamil and sulfamethoxazole derivatives.

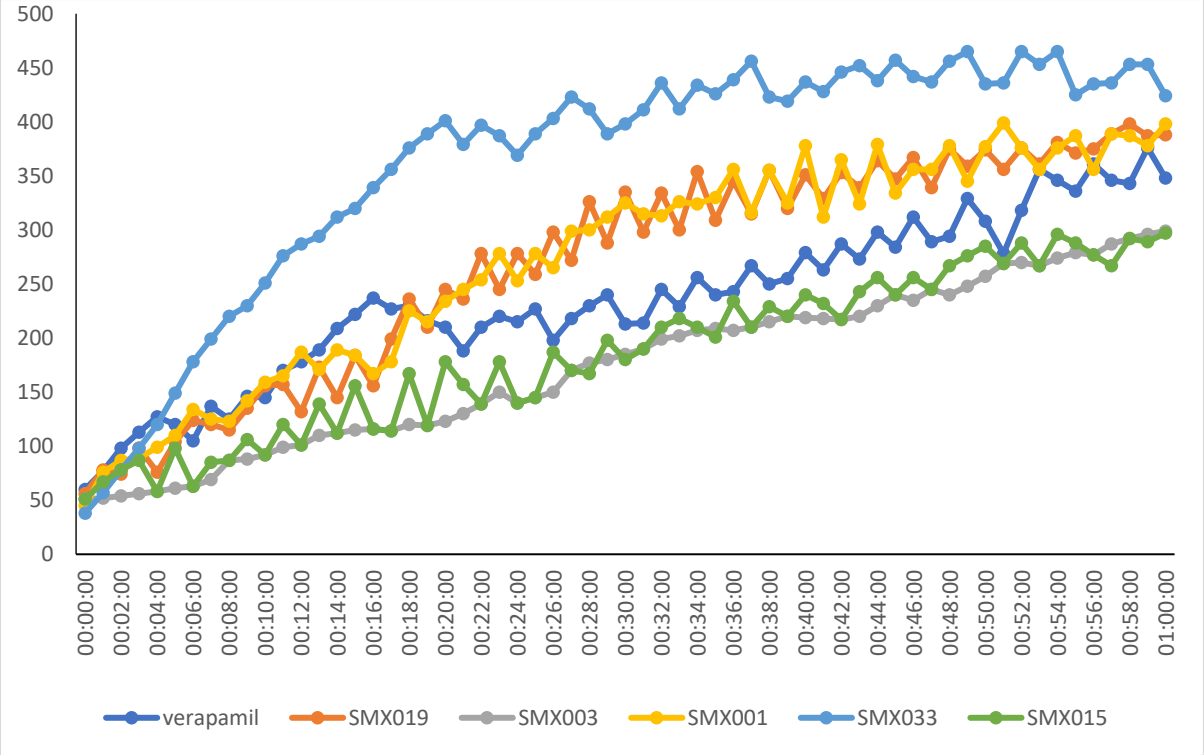

Figure 11d. Time-dependent efflux pump inhibition in *Salmonella typhi* by verapamil and sulfamethoxazole derivatives.

SMX033 was predicted to bind strongly in the periplasmic vestibule of AcrB, interacting with key residues such as Phe664 and Pro669 through significant van der Waals and hydrophobic interactions. The methyl group at the para position was computationally identified as essential for occupying the hydrophobic pocket formed by Phe664, a residue crucial for substrate binding and expulsion. By obstructing this vestibule, SMX033 is expected to stabilize AcrB in the "loose" (L) state, thereby preventing the conformational changes necessary for antibiotic export. The experimental observation of high ethidium bromide (EtBr) accumulation serves as direct functional evidence of this mechanism [77]. Additionally, the moderate to satisfactory efflux pump inhibitor (EPI) activity of SMX015, SMX019, SMX003, and SMX001 correlates with their in silico profiles. Their diverse substituents (ester, bromo, and nitro) were anticipated to interact with the vestibule through different mechanisms, such as forming hydrogen bonds with Arg717 or pi-sulfur interactions with Met575, which explains their measurable, albeit lower, efflux inhibition compared to SMX033 [78].

7.0 *Conclusion*

This study has successfully demonstrated a rational, integrated computational and experimental approach to design novel sulfamethoxazole derivatives that have potential to simultaneously target bacterial viability, virulence, and resistance mechanisms. Our structure-guided design yielded a focused library of derivatives, from which five candidates were prioritized based on superior predicted binding affinities towards DHPS, the quorum-sensing regulator LasR, and the efflux pump transporter AcrB. The synthesis of these compounds was achieved efficiently, and their structures were unequivocally confirmed via NMR and HRMS. Biological evaluation revealed potent, broad-spectrum antimicrobial activity (MICs 15.625–125 μg/mL) against key ESKAPE pathogens, with lead compounds **SMX033** and **SMX015** exhibiting exceptional potency. Crucially, the experimental data strongly correlated with our *in silico* predictions. The derivatives achieved near-complete biofilm inhibition (>99%) by disrupting LasR-mediated quorum sensing, and **SMX033** emerged as a potent efflux pump inhibitor, directly corroborating our AcrB binding models. Furthermore, the markedly low cytotoxicity of **SMX033** (CC_{50} = 286.20 μM) underscores its promising selective toxicity and potential as a therapeutic scaffold. This work provides compelling proof-of-concept for a multi-targeting strategy to overcome multidrug resistance. By inhibiting DHPS, LasR, and AcrB concurrently, these sulfamethoxazole derivatives can attack the pathogen on multiple fronts, thereby mitigating the evolutionary pressure that leads to resistance. The excellent correlation between our computational predictions and experimental results establishes a validated blueprint for the potential rational design of next-generation antimicrobial agents. Future work will focus on *in vivo* efficacy studies, further medicinal chemistry optimization to improve potency and aqueous solubility and expanding this strategy to a broader chemical space to combat the ever-growing threat of pan-drug-resistant infections.

8.0 Declaration of Competing Interest

The authors declare that they have no known competing financial interests or personal relationships that could have appeared to influence the work reported in this paper.

Appendix SM1-SM20: Supplementary data attached

The supplementary data on the synthesized compounds is attached.

9.0 Credit Authorship Contribution Statement

Cedric D.K. Amengor: Supervised the project, developed the overall conceptual framework, oversaw the synthesis, wrote the original draft, and proofread the manuscript.

Benedicta Yayra Adzah: Carried out the synthesis of the compounds

Prince Danan Biniyam: Designed the computational conceptual framework and methodology, authored the molecular docking and MMGBSA, and proofread the manuscript.

Ernest Oyeh, Vuvor Faustina and Yvonne Dogbeda Agboyibor assisted in the characterisation of the compounds.

Victoria O. Adu: Provided computational technical support for ADME analysis, assisted in data curation, and proofread the manuscript.

Michael Osei: Provided computational technical support for molecular docking, assisted in data curation, and proofread the manuscript.

Kwabena Adu-Adjei: Provided computational technical support for ADME analysis, assisted in data curation, and proofread the manuscript.

Patrick Gyan , En Zhang, Ampomah-Wireko: Contributed to the writing of the antitubercular section and proofread the manuscript.

Paul Quansah and Cyril Makafui Amengor: Provided mathematical and statistical support for antimicrobial data analysis.

Joshua Boateng: Interpreted the HRMS data and edited the first draft of the manuscript.

Victoria Elmes: Carried out the NMR analysis and provided technical expertise on the NMR instrumentation

Iain Goodall: Carried out the HRMS analysis and provided technical expertise on the Mass Spectrometer.

10.0 Acknowledgements

The authors would like to express their sincere gratitude to the technicians of the Synthetic Medicinal Chemistry and Computational Division at the School of Pharmacy, University of Health and Allied Sciences, for their invaluable support.

11.0 Data Availability Statement

The original contributions and data obtained in the study are presented in the article.

12.0 References

1. Xu, C., Kong, L., Gao, H., Cheng, X., & Wang, X. (2022). A review of current bacterial resistance to antibiotics in food animals. Frontiers in microbiology, 13, 822689.

2.High, K. P. (2004). Infection as a cause of age-related morbidity and mortality. Ageing Research Reviews, 3(1), 1-14.

3. Salam, M. A., Al-Amin, M. Y., Salam, M. T., Pawar, J. S., Akhter, N., Rabaan, A. A., & Alqumber, M. A. (2023, July). Antimicrobial resistance: a growing serious threat for global public health. In Healthcare (Vol. 11, No. 13, p. 1946). MDPI.

4. Taylor, A. P., Robinson, R. P., Fobian, Y. M., Blakemore, D. C., Jones, L. H., & Fadeyi, O. (2016). Modern advances in heterocyclic chemistry in drug discovery. Organic & biomolecular chemistry, 14(28), 6611-6637.

5. Jampilek, J. (2019). Heterocycles in medicinal chemistry. Molecules, 24(21), 3839.

6. Shabir, G., Saeed, A., Zahid, W., Naseer, F., Riaz, Z., Khalil, N., ... & Albericio, F. (2023). Chemistry and pharmacology of fluorinated drugs approved by the FDA (2016‐2022). Pharmaceuticals, 16(8), 1162.

7. Kumari, S., Carmona, A. V., Tiwari, A. K., & Trippier, P. C. (2020). Amide bond bioisosteres: Strategies, synthesis, and successes. Journal of medicinal chemistry, 63(21), 12290-12358.

8. Martis, G. J., & Gaonkar, S. L. (2025). Advances in isoxazole chemistry and their role in drug discovery. RSC advances, 15(11), 8213-8243.

9. Li, S., Mei, Y., Jiang, L., Yang, X., Zeng, W., & Du, Y. (2025). Oxazole and isoxazole-containing pharmaceuticals: targets, pharmacological activities, and their SAR studies. RSC Medicinal Chemistry.

10. Ramlakhan, S., Singh, V., Stone, J., & Ramtahal, A. (2014). Clinical options for the treatment of urinary tract infections in children. Clinical Medicine Insights: Pediatrics, 8, CMPed-S8100.

11. Sørum, H. (2005). Antimicrobial drug resistance in fish pathogens. Antimicrobial resistance in bacteria of animal origin, 213-238.

12. Jubeh, B., Breijyeh, Z., & Karaman, R. (2020). Resistance of gram-positive bacteria to current antibacterial agents and overcoming approaches. Molecules, 25(12), 2888.

13. Pervaiz, M., Riaz, A., Munir, A., Saeed, Z., Hussain, S., Rashid, A., ... & Adnan, A. (2020). Synthesis and characterization of sulfonamide metal complexes as antimicrobial agents. Journal of Molecular Structure, 1202, 127284.

14. Claudel, M., Schwarte, J. V., & Fromm, K. M. (2020). New antimicrobial strategies based on metal complexes. Chemistry, 2(4), 849-899.

15. Wang, S., Zhang, H. Y., Wang, L., Duan, Z. J., & Kennedy, I. (2006). Analysis of sulphonamide residues in edible animal products: A review. Food additives and contaminants, 23(4), 362-384.

16. Ballav, S., Jana, D., Guchhait, K. C., Das, B., Manna, M., Hazra, S., ... & Ghosh, C. (2023). Efflux Pumps and their role in the development of multi-drug resistant bacterial biofilm. In Biofilm Associated Antimicrobial Resistance and Its Recovery (pp. 66-81). CRC Press.

17. Alenazy, R. (2022). Antibiotic resistance in Salmonella: Targeting multidrug resistance by understanding efflux pumps, regulators and the inhibitors. Journal of King Saud University-Science, 34(7), 102275.

18. Scoffone, V. C., Trespidi, G., Barbieri, G., Irudal, S., Perrin, E., & Buroni, S. (2021). Role of RND efflux pumps in drug resistance of cystic fibrosis pathogens. Antibiotics, 10(7), 863.

19. Ghany, L. M. A., Ryad, N., Abdel-Aziz, M. S., Abd El-Lateef, H. M., Zaki, I., & Beshay, B. Y. (2024). Design, synthesis, antimicrobial evaluation, and molecular modeling of new sulfamethoxazole and trimethoprim analogs as potential DHPS/DHFR inhibitors. Journal of Molecular Structure, 1309, 138170.

20. Giordanetto, F., Fowler, P. W., Saqi, M., & Coveney, P. V. (2005). Large scale molecular dynamics simulation of native and mutant dihydropteroate synthase‐sulphanilamide complexes suggests the molecular basis for dihydropteroate synthase drug resistance. Philosophical Transactions of the Royal Society A: Mathematical, Physical and Engineering Sciences, 363(1833), 2055-2073.

21. Salubi, C. A. (2023). Molecular Docking Investigation and Pharmacokinetic Properties Prediction of Some Benzimidazole Analogues as Dihydropteroate Synthase (DHPS) Inhibitors.

22. Breijyeh, Z., & Karaman, R. (2023). Design and synthesis of novel antimicrobial agents. Antibiotics, 12(3), 628.

23. Hanai, T. (2009). Chromatography and computational chemical analysis for drug discovery. Frontiers in Medicinal Chemistry: Volume 4, 86-129.

24. Azevedo-Barbosa, H., do Vale, B. P., Guidolin Rossi, G., dos Santos Siqueira, F., Bordignon Guterres, K., de Campos, M. M. A., ... & Teixeira Carvalho, D. (2021). Design, Synthesis, Antimicrobial Evaluation and in Silico Studies of Eugenol-Sulfonamide Hybrids. Chemistry & Biodiversity, 18(5), e2100066.

25. Das, D., Sahu, N., Roy, S., Dutta, P., Mondal, S., Torres, E. L., & Sinha, C. (2015). The crystal structure of sulfamethoxazole, interaction with DNA, DFT calculation, and molecular docking studies. *Spectrochimica Acta Part A: Molecular and Biomolecular Spectroscopy*, *137*, 560-568.

26. . Fetse, J. P., Kyekyeku, J. O., Dueve, E., & Mensah, K. B. (2014). Wound healing activity of total alkaloidal extract of the root bark of Alstonia boonei (Apocynacea). British Journal of Pharmaceutical Research, 4(23), 2642.

27. .Agyare, C., Dwobeng, A. S., Agyepong, N., Boakye, Y. D., Mensah, K. B., Ayande, P. G., & Adarkwa-Yiadom, M. (2013). Antimicrobial, antioxidant, and wound healing properties of Kigelia africana (Lam.) Beneth. and Strophanthus hispidus DC. Advances in Pharmacological and Pharmaceutical Sciences, 2013(1), 692613.

28. . Wasfi, R., Abd El-Rahman, O. A., Mansour, L. E., Hanora, A. S., Hashem, A. M., & Ashour, M. S. (2012). Antimicrobial activities against biofilm formed by Proteus mirabilis isolates from wound and urinary tract infections. Indian journal of medical microbiology, 30(1), 76-80.

29. Adekola, H. A., Adeleye, A. O., Adesetan, T. O., Folorunso, J. B., & Odeyemi, F. A. (2022). Antibacterial Activity of Vanillic Acid against Staphylococcus aureus, Salmonella typhi, and Proteus mirabilis. Microbes, Infect Chemother, 2(12), 1-6.

30. Anokwah, D., Asante-Kwatia, E., Asante, J., Obeng-Mensah, D., Danquah, C. A., Amponsah, I. K., ... & Mensah, A. Y. (2023). Antibacterial, Resistance Modulation, Anti-Biofilm Formation, and Efflux Pump Inhibition Properties of Loeseneriella africana (Willd.) N. Halle (Celastraceae) Stem Extract and Its Constituents. Microorganisms, 12(1), 7.

31.. Mowla, R., Wang, Y., Ma, S., & Venter, H. (2018). Kinetic analysis of the inhibition of the drug efflux protein AcrB using surface plasmon resonance. Biochimica et Biophysica Acta (BBA)-Biomembranes, 1860(4), 878-886.

32. Azeem, K., Fatima, S., Ali, A., Ubaid, A., Husain, F. M., & Abid, M. (2025). Biochemistry of bacterial biofilm: insights into antibiotic resistance mechanisms and therapeutic intervention. Life, 15(1), 49.

33 He, X., Liu, S., Lee, T. S., Ji, B., Man, V. H., York, D. M., & Wang, J. (2020). Fast, accurate, and reliable protocols for routine calculations of protein–ligand binding affinities in drug design projects using AMBER GPU-TI with ff14SB/GAFF. ACS omega, 5(9), 4611-4619.

34. Bhadra, P., & Siu, S. W. (2019). Refined empirical force field to model protein–self-assembled monolayer interactions based on AMBER14 and GAFF. Langmuir, 35(29), 9622-9633.

35. Grabski, H., Hunanyan, L., Tiratsuyan, S., & Vardapetyan, H. (2019). Interaction of N-3-oxododecanoyl homoserine lactone with transcriptional regulator LasR of Pseudomonas aeruginosa: Insights from molecular docking and dynamics simulations. F1000Research, 8, 324.

36. Callil-Soares, P. H., Biasi, L. C. K., & Pessoa Filho, P. D. A. (2023). Effect of preprocessing and simulation parameters on the performance of molecular docking studies. Journal of Molecular Modeling, 29(8), 251.

37. Reynolds, C. H., Bembenek, S. D., & Tounge, B. A. (2007). The role of molecular size in ligand efficiency. Bioorganic & medicinal chemistry letters, 17(15), 4258-4261.

38. Murray, C. W., Erlanson, D. A., Hopkins, A. L., Keserü, G. M., Leeson, P. D., Rees, D. C., ... & Richmond, N. J. (2014). Validity of ligand efficiency metrics. ACS medicinal chemistry letters, 5(6), 616-618.

39. Singh, N., & Warshel, A. (2010). Absolute binding free energy calculations: On the accuracy of computational scoring of protein–ligand interactions. Proteins: Structure, Function, and Bioinformatics, 78(7), 1705-1723.

40. Putri, R. F., Abdjan, M. I., Santosaningsih, D., Ni, Y. L., Putri, N., Khairunnisa, F., ... & Baktir, (2025). Molecular Dynamic and Docking Simulation in Exploring a Potential Extracellular Matrix-Based Antibiofilm: Fighting the Resistant Pseudomonas aeruginosa-Candida albicans. Engineered Science, 34, 1386.

41. Martis, G. J., & Gaonkar, S. L. (2025). Advances in isoxazole chemistry and their role in drug discovery. RSC advances, 15(11), 8213-8243.

42. Subbaiah, M. A., & Meanwell, N. A. (2021). Bioisosteres of the phenyl ring: recent strategic applications in lead optimization and drug design. Journal of Medicinal Chemistry, 64(19), 14046-14128.

43. Marsault, E., & Peterson, M. L. (2011). Macrocycles are great cycles: applications, opportunities, and challenges of synthetic macrocycles in drug discovery. Journal of medicinal chemistry, 54(7), 1961-2004.

44. Coe, K. J. (2008). Metabolism and cytotoxicity of the nitroaromatic drug Flutamide and its cyano analog in hepatocyte cell lines. University of Washington.

45. Saran, C., & Brouwer, K. L. (2023). Hepatic bile acid transporters and drug-induced hepatotoxicity. Toxicologic pathology, 51(7-8), 405-413.

46. Wang, Z., Sun, H., Yao, X., Li, D., Xu, L., Li, Y., ... & Hou, T. (2016). Comprehensive evaluation of ten docking programs on a diverse set of protein–ligand complexes: the prediction accuracy of sampling power and scoring power. Physical Chemistry Chemical Physics, 18(18), 12964-12975.

47. Jakhar, R., Dangi, M., Khichi, A., & Chhillar, A. K. (2020). Relevance of molecular docking studies in drug designing. Current Bioinformatics, 15(4), 270-278.

48. Bakheit, A. H., Attwa, M. W., Kadi, A. A., Ghabbour, H. A., & Alkahtani, H. M. (2023). Exploring the chemical reactivity, molecular docking, molecular dynamic simulation and ADMET properties of a tetrahydrothienopyridine derivative using computational methods. Crystals, 13(7), 1020.

49. Nissink, J. W. M., & Degorce, S. (2013). Analyzing compound and project progress through multi-objective-based compound quality assessment. Future Medicinal Chemistry, 5(7), 753-767.

50. Salubi, C. A. (2023). Molecular Docking Investigation and Pharmacokinetic Properties Prediction of Some Benzimidazole Analogues as Dihydropteroate Synthase (DHPS) Inhibitors.

51. Bourne, C. R. (2014). Utility of the biosynthetic folate pathway for targets in antimicrobial discovery. Antibiotics, 3(1), 1-28.

52. Nalam, M. N., Ali, A., Altman, M. D., Reddy, G. S., Chellappan, S., Kairys, V., Ozen, A., Cao, H., Gilson, M. K., Tidor, B., Rana, T. M., & Schiffer, C. A. (2010). Evaluating the substrate-

envelope hypothesis: structural analysis of novel HIV-1 protease inhibitors designed to be robust against drug resistance. Journal of virology, 84(10), 5368–5378.

53. Ayers, K. A. (2009). Structural and kinetics studies of the enzyme dihydropteroate synthase and the implications for antibiotic resistance. The University of Tennessee Health Science Center.

54. Genheden, S., & Ryde, U. (2015). The MM/PBSA and MM/GBSA methods to estimate ligand-binding affinities. Expert opinion on drug discovery, 10(5), 449-461.

55. Zürcher, M., & Diederich, F. (2008). Structure-based drug design: exploring the proper filling of apolar pockets at enzyme active sites. The Journal of organic chemistry, 73(12), 4345-4361.

56. Zhou, H. X., & Pang, X. (2018). Electrostatic interactions in protein structure, folding, binding, and condensation. Chemical reviews, 118(4), 1691-1741.

57. Shah, M., Taylor, V. L., Bona, D., Tsao, Y., Stanley, S. Y., Pimentel-Elardo, S. M., ... & Maxwell, K. L. (2021). A phage-encoded anti-activator inhibits quorum sensing in Pseudomonas aeruginosa. Molecular Cell, 81(3), 571-583.

58. Di Fruscia, P., Carbone, A., Bottegoni, G., Berti, F., Giacomina, F., Ponzano, S., ... & Bertozzi, F. (2021). Discovery and SAR evolution of pyrazole azabicyclo [3.2. 1] octane sulfonamides as a novel class of non-covalent N-Acylethanolamine-Hydrolyzing acid amidase (NAAA) inhibitors for oral administration. Journal of Medicinal Chemistry, 64(18), 13327-13355.

59. Drew, D., Klepsch, M. M., Newstead, S., Flaig, R., De Gier, J. W., Iwata, S., & Beis, K. (2008). The structure of the efflux pump AcrB in complex with bile acid. Molecular membrane biology, 25(8), 677-682.

60. Bibens, L., Becker, J. P., Dassonville-Klimpt, A., & Sonnet, P. (2023). A review of fatty acid biosynthesis enzyme inhibitors as promising antimicrobial drugs. Pharmaceuticals, 16(3), 425.

61. Mehla, J., Malloci, G., Mansbach, R., López, C. A., Tsivkovski, R., Haynes, K., ... & Zgurskaya, H. I. (2021). Predictive rules of efflux inhibition and avoidance in Pseudomonas aeruginosa. MBio, 12(1), 10-1128.

62. Baym, M., Stone, L. K., & Kishony, R. (2016). Multidrug evolutionary strategies to reverse antibiotic resistance. Science, 351(6268), aad3292.

63. Flemming, H. C., & Wingender, J. (2010). The biofilm matrix. Nature reviews microbiology, 8(9), 623-633.

64. Rabin, N., Zheng, Y., Opoku-Temeng, C., Du, Y., Bonsu, E., & Sintim, H. O. (2015). Biofilm formation mechanisms and targets for developing antibiofilm agents. Future medicinal chemistry, 7(4), 493-512.

65. Singh, S., Datta, S., Narayanan, K. B., & Rajnish, K. N. (2021). Bacterial exo-polysaccharides in biofilms: role in antimicrobial resistance and treatments. Journal of Genetic Engineering and Biotechnology, 19(1), 140.

66. Elawady, R., Aboulela, A. G., Gaballah, A., Ghazal, A. A., & Amer, A. N. (2024). Antimicrobial Sub-MIC induces Staphylococcus aureus biofilm formation without affecting the bacterial count. BMC infectious diseases, 24(1), 1065.

67. Wang, X., Liu, M., Yu, C., Li, J., & Zhou, X. (2023). Biofilm formation: mechanistic insights a5d therapeutic targets. Molecular biomedicine, 4(1), 49.

68. Skogman, M. E., Vuorela, P. M., & Fallarero, A. (2012). Combining biofilm matrix measurements with biomass and viability assays in susceptibility assessments of antimicrobials against Staphylococcus aureus biofilms. The Journal of antibiotics, 65(9), 453-459.

69. Gaurav, A., Bakht, P., Saini, M., Pandey, S., & Pathania, R. (2023). Role of bacterial efflux pumps in antibiotic resistance, virulence, and strategies to discover novel efflux pump inhibitors. Microbiology, 169(5), 001333.

70. AlMatar, M., Albarri, O., Makky, E. A., & Köksal, F. (2021). Efflux pump inhibitors: new updates. Pharmacological Reports, 73(1), 1-16.

71. Huang, L., Wu, C., Gao, H., Xu, C., Dai, M., Huang, L., ... & Cheng, G. (2022). Bacterial multidrug efflux pumps at the frontline of antimicrobial resistance: an overview. Antibiotics, 11(4), 520.

72. Lamut, A., Peterlin Mašič, L., Kikelj, D., & Tomašič, T. (2019). Efflux pump inhibitors of clinically relevant multidrug resistant bacteria. Medicinal Research Reviews, 39(6), 2460-2504.

73. Zhang, L., Tian, X., Sun, L., Mi, K., Wang, R., Gong, F., & Huang, L. (2024). Bacterial efflux pump inhibitors reduce antibiotic resistance. Pharmaceutics, 16(2), 170.

74. Nafisi, S., Saboury, A. A., Keramat, N., Neault, J. F., & Tajmir-Riahi, H. A. (2007). Stability and structural features of DNA intercalation with ethidium bromide, acridine orange and methylene blue. Journal of Molecular Structure, 827(1-3), 35-43.

75. Pal, S., Misra, A., Banerjee, S., & Dam, B. (2020). Adaptation of ethidium bromide fluorescence assay to monitor activity of efflux pumps in bacterial pure cultures or mixed population from environmental samples. Journal of King Saud University-Science, 32(1), 939-945.

76. Limaverde, P. W., Campina, F. F., da Cunha, F. A., Crispim, F. D., Figueredo, F. G., Lima, L. F., ... & Tintino, S. R. (2017). Inhibition of the TetK efflux-pump by the essential oil of Chenopodium ambrosioides L. and α-terpinene against Staphylococcus aureus IS-58. Food and chemical toxicology, 109, 957-961.

77. Tintino, S. R., Oliveira-Tintino, C. D., Campina, F. F., Weslley Limaverde, P., Pereira, P. S., Siqueira-Junior, J. P., ... & Balbino, V. Q. (2018). Vitamin K enhances the effect of antibiotics inhibiting the efflux pumps of Staphylococcus aureus strains. Medicinal Chemistry Research, 27(1), 261-267.

78. Olmsted III, J., & Kearns, D. R. (1977). Mechanism of ethidium bromide fluorescence enhancement on binding to nucleic acids. Biochemistry, 16(16), 3647-3654.

79. Olender, D., Żwawiak, J., & Zaprutko, L. (2018). Multidirectional efficacy of biologically active nitro compounds included in medicines. Pharmaceuticals, 11(2), 54.